

Critical free energy and Casimir forces in rectangular geometries

Volker Dohm

Institute for Theoretical Physics, RWTH Aachen University, D-52056 Aachen, Germany

(Received 30 December 2010; published 4 August 2011)

We study the critical behavior of the free energy and the thermodynamic Casimir force in a $L_{\parallel}^{d-1} \times L$ block geometry in $2 < d < 4$ dimensions with aspect ratio $\rho = L/L_{\parallel}$ on the basis of the $O(n)$ symmetric φ^4 lattice model with periodic boundary conditions and with isotropic short-range interactions. Exact results are derived in the large- n limit describing the geometric crossover from film ($\rho = 0$) over cubic ($\rho = 1$) to cylindrical ($\rho = \infty$) geometries. For $n = 1$, three perturbation approaches in the minimal renormalization scheme at fixed d are presented that cover both the central finite-size regime near T_c for $1/4 \lesssim \rho \lesssim 3$ and the region well above and below T_c . At bulk T_c , we predict the critical Casimir force in the vertical (L) direction to be negative (attractive) for a slab ($\rho < 1$), positive (repulsive) for a rod ($\rho > 1$), and zero for a cube ($\rho = 1$). Our results for finite-size scaling functions agree well with Monte Carlo data for the three-dimensional Ising model by Hasenbusch for $\rho = 1$ and by Vasilyev *et al.* for $\rho = 1/6$ above, at, and below T_c .

DOI: [10.1103/PhysRevE.84.021108](https://doi.org/10.1103/PhysRevE.84.021108)

PACS number(s): 05.70.Jk, 64.60.-i, 75.40.-s

I. INTRODUCTION AND OVERVIEW

In the theory of finite-size effects near phase transitions, the study of critical Casimir forces [1] has remained on a highly active level over the past two decades [2]. Close to criticality and for sufficiently large confining lengths, such forces are predicted to exhibit universal features in the sense that, for *isotropic* systems with short-range interactions, their scaling functions depend only on the geometric shape, on the boundary conditions (BC), and on the universality class of the system. For *anisotropic* systems of the same universality class (e.g., lattice systems with noncubic symmetry such as anisotropic superconductors [3]), however, two-scale factor universality [4] is absent [5–10] and the critical Casimir forces are nonuniversal as they depend on the lattice structure and on the microscopic couplings through a matrix of nonuniversal anisotropy parameters. This implies that the Casimir amplitudes at bulk T_c depend, in general, on $d(d+1)/2 - 1$ nonuniversal parameters in d -dimensional anisotropic systems with given shape and given BC [5–9]. This prediction is readily testable by Monte Carlo (MC) simulations of anisotropic spin models; it was also noted in [7] that experiments in anisotropic superconducting films [3] could, in principle, demonstrate the nonuniversality of the critical Casimir force [11]. A corresponding nonuniversality of the Binder cumulant [4,17] has been predicted [5,7] and has been confirmed by MC simulations for the anisotropic Ising model [18].

In this paper, the focus is on isotropic systems with periodic BC for the ($n = 1$) Ising universality class on the basis of the $O(n)$ symmetric φ^4 lattice model.

Theoretical studies (beyond mean-field theory) of the Casimir force in such systems have been restricted to $\infty^{d-1} \times L$ (film) geometry within the $\varepsilon = 4 - d$ expansion above and at T_c [19–21]. The most interesting region, however, is the region *below* T_c where the scaling function of the Casimir force displays a characteristic minimum as detected by MC simulations [16,22]. A basic difficulty in treating an infinite film system (for $n = 1$) below T_c is the existence of a film transition at a separate critical temperature $T_{c,\text{film}} < T_c$ just in the region of the minimum of the Casimir force [23]. A quantitative theory of the corresponding dimensional crossover between different

critical behavior of the d -dimensional bulk transition at T_c and the $d - 1$ dimensional film transition at $T_{c,\text{film}}$ constitutes an as yet unsolved problem, except for the case of the Gaussian model [8].

In this paper, we circumvent the problem of dimensional crossover by studying a *finite* $L_{\parallel}^{d-1} \times L$ block geometry with finite aspect ratio $\rho = L/L_{\parallel}$ [24]. This geometry includes slab ($0 < \rho < 1$), cubic ($\rho = 1$), and rodlike ($\rho > 1$) geometries (Fig. 1). The practical relevance of the slab geometry is based on the facts (i) that all experiments and all MC simulations have necessarily been performed at finite ρ rather than at $\rho = 0$, (ii) that the shape of the finite-size scaling function of the Casimir force depends on the aspect ratio ρ only weakly in the regime $\rho \ll 1$ [16,22], and (iii) that the singularity of the free energy and the Casimir force at $T_{c,\text{film}}$ for $\rho = 0$ is only very weak, such that recent MC data [16] could not detect this singularity. (By contrast, the logarithmic divergence of the specific heat for $\rho = 0$ near $T_{c,\text{film}}$ should be well detectable.) This justifies the description of the main features of the film system above and below T_c , to a good approximation, by a finite slab geometry with small but finite aspect ratio. As an interesting by-product of our theory, the dependence on the aspect ratio for larger ρ is obtained, which permits us to describe the geometric crossover from slab ($\rho \ll 1$) over cubic ($\rho = 1$) to rodlike ($\rho \gg 1$) geometries. The geometric crossover from block to cylindrical ($\rho = \infty$) geometries has been studied earlier near first-order transitions by Privman and Fisher [25]. In this context, we note that systems with $\rho \gg 1$ are of experimental interest in the area of finite-size effects near the superfluid transition of ^4He [26,27]. Furthermore, finite-size theories for block geometries are directly testable by MC simulations.

The finite-block system is conceptually simpler than the infinite film system because of a considerable technical advantage: For finite $0 < \rho < \infty$, the system has a discrete mode spectrum with only one single lowest mode, in contrast to the more complicated situation of a lowest-mode *continuum* in film ($\rho = 0$) or cylinder ($\rho = \infty$) geometry. This opens up the opportunity of building upon the advances that have been achieved in the description of finite-size effects in systems that are finite in all directions [7,28–31]. It is not clear *a priori*,

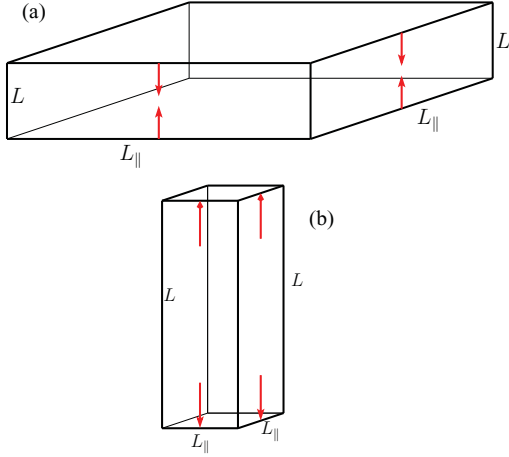


FIG. 1. (Color online) Three-dimensional $L_{\parallel}^2 \times L$ block geometries with aspect ratio $\rho = L/L_{\parallel}$: (a) slab ($\rho < 1$), (b) rod ($\rho > 1$). Arrows: critical Casimir force (2.15). Our theory (in Secs. III–V) predicts that, for isotropic systems with periodic BC and short-range interactions, $F_{\text{Casimir},s}$ at bulk T_c is negative (attractive) for a slab, positive (repulsive) for a rod, and zero for a cube ($\rho = 1$).

however, in what range of ρ such a theory is reliable since, ultimately, for sufficiently small $\rho \ll 1$ or sufficiently large $\rho \gg 1$, the concept of separating a single lowest mode must break down. Therefore, as a crucial part of our theory, it is necessary to provide quantitative evidence for the expected range of applicability of our theory at finite ρ . This is one of the reasons why we also consider (in Sec. III) the large- n limit, the exact results of which turn out to be helpful in estimating the range of validity of our approximate results for $n = 1$.

As we shall present *three* different perturbation approaches with different ranges of applicability for the case $n = 1$, we give here a brief overview of our strategy. The basic physical quantity is the singular part of the excess free energy density f_s^{ex} . On the basis of previous work [7,32], it is expected that, for our isotropic system with a finite volume $L_{\parallel}^{d-1} \times L$, there exist three different regimes (a), (b), and (c) for the finite-size critical behavior of the excess free energy f_s^{ex} . These different regimes correspond to the three regions in Fig. 2 that are separated by the dashed lines:

(a) The regime well above T_c that includes an exponential size dependence $f_s^{\text{ex}} \sim \exp(-L/\xi_{e+})$ or $f_s^{\text{ex}} \sim \exp(-L_{\parallel}/\xi_{e+})$ for large $L/\xi_{e+} \gg 1$ and $L_{\parallel}/\xi_{e+} \gg 1$, with ξ_{e+} being the exponential (“true”) bulk correlation length [7,33,34] above T_c ; in this regime, f_s^{ex} is expected to tend to zero in the high-temperature limit at finite L and L_{\parallel} or in the limit of large L and L_{\parallel} at fixed temperature $T > T_c$.

(b) The central finite-size regime near T_c that includes the power-law behavior $f_s^{\text{ex}} \sim L^{-d}$ or $f_s^{\text{ex}} \sim L_{\parallel}^{-d}$ for large L at fixed L/ξ_{\pm} , $0 \leq L/\xi_{\pm} \leq O(1)$ and for large L_{\parallel} at fixed L_{\parallel}/ξ_{\pm} , $0 \leq L_{\parallel}/\xi_{\pm} \leq O(1)$ above, at, and below T_c , where ξ_{\pm} is the second-moment bulk correlation length.

(c) The regime well below T_c that includes an exponential size dependence $\sim \exp(-L/\xi_{e-})$ or $\sim \exp(-L_{\parallel}/\xi_{e-})$ for large $L/\xi_{e-} \gg 1$ and $L_{\parallel}/\xi_{e-} \gg 1$ with ξ_{e-} being the exponential (“true”) bulk correlation length [7,33,34] below T_c ; in this

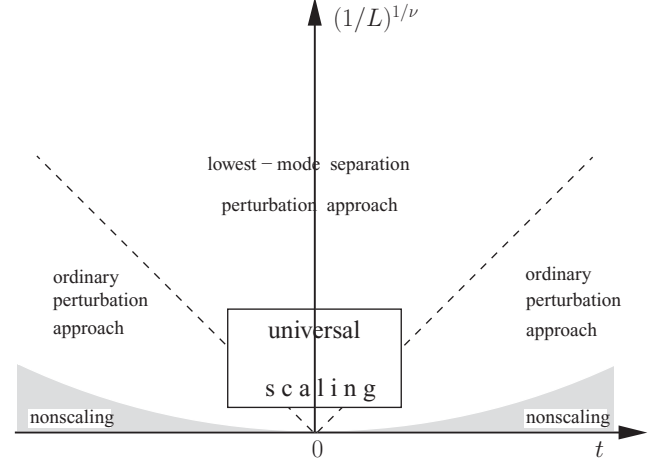


FIG. 2. Schematic plot of the asymptotic part of the $L^{-1/\nu} - t$ plane, with $t \equiv (T - T_c)/T_c$, for the φ^4 model with $n = 1$ and with isotropic interactions on a simple-cubic lattice with lattice spacing \tilde{a} in a $L_{\parallel}^{d-1} \times L$ block geometry with periodic boundary conditions and finite aspect ratio $\rho = L/L_{\parallel}$. In the central finite-size region (above the dashed lines), the lowest mode must be separated, whereas, outside this region (below the dashed lines), ordinary perturbation theory is applicable. Above the shaded region, universal finite-size scaling is valid for isotropic systems. In the large- L regime at $t \neq 0$ (shaded region), the exponential form of the size dependence violates both finite-size scaling and universality because of a non-negligible dependence on the lattice spacing \tilde{a} . An analogous plot applies to the $L_{\parallel}^{-1/\nu} - t$ plane.

regime, f_s^{ex} is expected to have an exponential decay toward a *finite* value $-V^{-1} \ln 2$ in the low-temperature limit at finite volume V [32] and to tend to zero in the limit of large volume at fixed temperature $T < T_c$.

For a description of the cases (a) and (c), ordinary perturbation theory with respect to the four-point coupling u_0 of the φ^4 theory is sufficient. This ordinary perturbation approach is applicable to the regions below the dashed lines in Fig. 2. This approach will be presented in Sec. VI. For the case (b), a separation of the lowest mode and a perturbation treatment of the higher modes is necessary [7,28–31]. This approach is applicable to the region between the dashed lines in Fig. 2, which we refer to as the *central finite-size regime*. In Secs. IV and V, we treat the case (b) in $2 < d < 4$ dimensions on the basis of the φ^4 lattice model in the minimal renormalization scheme at fixed dimension d [35]. We consider a simple-cubic lattice with isotropic short-range interactions. We shall demonstrate that our different perturbation approaches complement each other and that the corresponding results match reasonably well at intermediate values of the scaling variables. As will be shown in Secs. V and VI, these results agree well with Monte Carlo data for the three-dimensional Ising model by Hasenbusch for $\rho = 1$ [36] and by Vasilyev *et al.* for $\rho = 1/6$ [16] above, at, and below T_c .

We shall see that in all regimes (a)–(c), universal finite-size scaling [37] of isotropic systems is valid, except for the regions that are indicated by the shaded areas in Fig. 2, where the exponential form of the size dependence violates both finite-size scaling and universality because of a non-negligible dependence on the lattice spacing \tilde{a} . The boundaries of the

shaded areas are not sharply defined; they are approximately determined by $L \simeq 24\xi_{\pm}^3/\tilde{a}^2$. This issue will be discussed in Sec. VI D.

II. MODEL AND BASIC DEFINITIONS

We start from the $O(n)$ symmetric φ^4 lattice Hamiltonian divided by $k_B T$:

$$H = \tilde{a}^d \left[\sum_{i=1}^N \left(\frac{r_0}{2} \varphi_i^2 + u_0 (\varphi_i^2)^2 \right) + \sum_{i,j=1}^N \frac{K_{i,j}}{2} (\varphi_i - \varphi_j)^2 \right], \quad (2.1)$$

$$r_0(T) = r_{0c} + a_0 t, \quad t = (T - T_c)/T_c, \quad (2.2)$$

with $a_0 > 0$, $u_0 > 0$ where T_c is the *bulk* critical temperature. The variables $\varphi_i \equiv \varphi(\mathbf{x}_i)$ are n -component vectors that represent the internal degrees of freedom of N particles on N lattice points \mathbf{x}_i of a d -dimensional simple-cubic lattice with lattice constant \tilde{a} and with periodic boundary conditions. The components $\varphi_i^{(\mu)}$, $\mu = 1, 2, \dots, n$ of φ_i , vary in the continuous range $-\infty \leq \varphi_i^{(\mu)} \leq \infty$. We consider a finite rectangular $L_{\parallel}^{d-1} \times L$ block geometry of volume $V = L_{\parallel}^{d-1} L$ with the aspect ratio

$$\rho = \frac{L}{L_{\parallel}}. \quad (2.3)$$

This block geometry includes the shape of a cube ($\rho = 1$), of a finite slab ($0 < \rho < 1$), and of a finite rod ($1 < \rho < \infty$) (Fig. 1).

The free energy per component and per unit volume divided by $k_B T$ is

$$f(t, L, L_{\parallel}) = -(nV)^{-1} \ln Z(t, L, L_{\parallel}), \quad (2.4)$$

where

$$Z(t, L, L_{\parallel}) = \left[\prod_{i=1}^N \frac{\int d^n \varphi_i}{\tilde{a}^{n(2-d)/2}} \right] \exp(-H) \quad (2.5)$$

is the dimensionless partition function. The bulk free energy density per component divided by $k_B T$ is obtained by

$$f_b(t) = \lim_{L \rightarrow \infty} \lim_{L_{\parallel} \rightarrow \infty} f(t, L, L_{\parallel}). \quad (2.6)$$

The *film* free energy density per component divided by $k_B T$ is obtained by taking the limit $L_{\parallel} \rightarrow \infty$ at fixed finite L (i.e., $\rho \rightarrow 0$):

$$f_{\text{film}}(t, L) = \lim_{L_{\parallel} \rightarrow \infty} f(t, L, L_{\parallel}), \quad (2.7)$$

corresponding to an $\infty^{d-1} \times L$ geometry. Our model also includes the limit $L \rightarrow \infty$ at fixed finite L_{\parallel} (i.e., $\rho \rightarrow \infty$) corresponding to an $L_{\parallel}^{d-1} \times \infty$ geometry, which we shall refer to as cylinder geometry

$$f_{\text{cyl}}(t, L_{\parallel}) = \lim_{L \rightarrow \infty} f(t, L, L_{\parallel}). \quad (2.8)$$

The excess free energy density per component divided by $k_B T$ is

$$f^{\text{ex}}(t, L, L_{\parallel}) = f(t, L, L_{\parallel}) - f_b(t). \quad (2.9)$$

For the finite $L_{\parallel}^{d-1} \times L$ system, we define the Casimir force per unit area and per component in the d th (vertical) direction (Fig. 1) as

$$F_{\text{Casimir}}(t, L, L_{\parallel}) = - \frac{\partial [L f^{\text{ex}}(t, L, L_{\parallel})]}{\partial L}, \quad (2.10)$$

where the derivative is taken at fixed L_{\parallel} . There exist, of course, also Casimir forces in the $d - 1$ horizontal directions. Our approach is well suited to calculate such forces. This will not be performed in this paper.

An important simplification of our model Hamiltonian (2.1) is the assumption of a rigid lattice with a rigid rectangular shape representing an idealized model system with a vanishing compressibility. The same assumption is made in lattice models on which previous Monte Carlo simulations of the Casimir force are based (see [2,12,16]). As a consequence, the number N of particles and the length L are directly related by $N = L_{\parallel}^{d-1} L / \tilde{a}^d$. Thus, the derivative with respect to L (at fixed L_{\parallel} , fixed \tilde{a} , and at fixed couplings K_{ij} and u_0) in (2.10) is equivalent to a derivative with respect to the number of horizontal layers of the lattice, i.e., number of particles. Such a definition of the Casimir force is appropriate when the ordering degrees of freedom (particles in fluid films [2,12,16] or Cooper pairs in superconducting films [3]) can move in and out of the film system without significantly changing the mean interparticle distance in the system. The definition (2.10) is, however, not appropriate for systems with a *fixed* number of ordering degrees of freedom. It appears that this is the reason why it was claimed in [12] that the Casimir force “is not a measurable quantity for magnets.” For similar claims, see [38]. There exist, however, long-ranged critical fluctuations of *elastic* degrees of freedom coupled to the order parameter in condensed matter systems with a finite compressibility (such as magnetic materials [13], alloys [15], and solids with structural phase transitions [14]), which give rise to L -dependent critical Casimir forces that are not contained in a description based on rigid-lattice models of the type (2.1). A description of such thermodynamic Casimir forces is provided by coupling the variables φ_i in (2.1) to the elastic degrees of freedom [13,15,39], in which case the free energy density $f(t, L, L_{\parallel}, N)$ depends on both the length L and the number N of particles as *independent* thermodynamic variables. Such a model is relevant for the calculation of an L -dependent elastic response to the critical Casimir force (e.g., an L -dependent contribution to magnetostriction). In the case of a compressible system, the number N of particles of which is fixed, the L -dependent thermodynamic Casimir force is given by

$$F_{\text{Casimir}}(t, L, L_{\parallel}, N) = - \frac{\partial [L f^{\text{ex}}(t, L, L_{\parallel}, N)]}{\partial L}, \quad (2.11)$$

where now the derivative is taken at fixed t , L_{\parallel} , and N . In such systems, anisotropy effects on the critical Casimir force are expected to play an important role. Equation (2.11) complements our arguments presented in [11]. As we consider the thermodynamic Casimir effect as a *finite-size* effect, our definition (2.11) does not include the bulk part of the total thermodynamic force $-\partial [L f(t, L, L_{\parallel}, N)] / \partial L$, which may give rise to measurable elastic bulk effects (such as a bulk contribution, e.g., to magnetostriction). Here, we shall not further discuss this extension to systems with a finite

compressibility, which is beyond the scope of this paper, the focus of which is on isotropic incompressible systems.

For small $|t|$, the bulk free energy density (2.6) can be uniquely decomposed into singular and nonsingular parts

$$f_b(t) = f_{b,s}(t) + f_{b,ns}(t). \quad (2.12)$$

For large L/\tilde{a} , L_\parallel/\tilde{a} , and small $|t|$, a corresponding assumption is made [4] for

$$f(t, L, L_\parallel) = f_s(t, L, L_\parallel) + f_{ns}(t, L, L_\parallel) \quad (2.13)$$

and for the excess free energy

$$f^{ex}(t, L, L_\parallel) = f_s^{ex}(t, L, L_\parallel) + f_{ns}^{ex}(t, L, L_\parallel), \quad (2.14)$$

where $f_{ns}(t, L, L_\parallel)$ and $f_{ns}^{ex}(t, L, L_\parallel)$ are regular functions of t and where $f_{ns}(t, L, L_\parallel)$ remains regular in the bulk limit $f_{ns}(t, L, L_\parallel) \rightarrow f_{b,ns}(t)$, whereas $f_s(t, L, L_\parallel) \rightarrow f_{b,s}(t)$ becomes singular in this limit. It has been assumed [37] that, for periodic BC, $f_{ns}(t, L, L_\parallel)$ is independent of L and L_\parallel , i.e., that it is identical with the regular bulk part $f_{b,ns}(t)$ of $f_b(t)$. We do not know of a general proof of this property; it appears to be valid for the φ^4 theory in the presence of short-range interactions $K_{i,j}$ but not in the presence of long-range correlations [7]. The critical behavior of F_{Casimir} can be calculated from its singular part

$$F_{\text{Casimir},s}(t, L, L_\parallel) = -\frac{\partial [L f_s^{ex}(t, L, L_\parallel)]}{\partial L}. \quad (2.15)$$

For the φ^4 lattice model with the interaction given in (2.19) below, it is expected that $f_{ns}^{ex}(t, L, L_\parallel) = 0$, thus, $F_{\text{Casimir}} = F_{\text{Casimir},s}$, which is consistent with our results in Secs. III–VI [see also the remark after Eq. (4.36) of [7]].

Our main goal is to study the case $n = 1$ at fixed finite aspect ratio $0 < \rho < \infty$, including extrapolations to the film and cylinder geometries. For comparison and as a guide for our extrapolations, we shall also consider the exactly solvable limit $n \rightarrow \infty$.

For periodic boundary conditions, the Fourier representations are

$$\varphi(\mathbf{x}_j) = V^{-1} \sum_{\mathbf{k}} e^{i\mathbf{k} \cdot \mathbf{x}_j} \hat{\varphi}(\mathbf{k}) \quad (2.16)$$

and

$$K_{i,j} = K(\mathbf{x}_i - \mathbf{x}_j) = N^{-1} \sum_{\mathbf{k}} e^{i\mathbf{k} \cdot (\mathbf{x}_i - \mathbf{x}_j)} \hat{K}(\mathbf{k}), \quad (2.17)$$

where the summations $\sum_{\mathbf{k}}$ run over N discrete vectors $\mathbf{k} \equiv (k_1, k_2, \dots, k_d)$ with Cartesian components $k_\alpha = 2\pi m_\alpha / L_\parallel$, $\alpha = 1, 2, \dots, d-1$, and $k_d = 2\pi m_d / L$, $m_\beta = 0, \pm 1, \pm 2, \dots$, in the range $-\pi/\tilde{a} \leq k_\beta < \pi/\tilde{a}$, $\beta = 1, \dots, d$. In terms of the Fourier components, the Hamiltonian reads as

$$H = V^{-1} \sum_{\mathbf{k}} \frac{1}{2} [r_0 + \delta \hat{K}(\mathbf{k})] \hat{\varphi}(\mathbf{k}) \hat{\varphi}(-\mathbf{k}) + u_0 V^{-3} \sum_{\mathbf{k}, \mathbf{p}, \mathbf{q}} [\hat{\varphi}(\mathbf{k}) \hat{\varphi}(\mathbf{p})] [\hat{\varphi}(\mathbf{q}) \hat{\varphi}(-\mathbf{k} - \mathbf{p} - \mathbf{q})], \quad (2.18)$$

where $\delta \hat{K}(\mathbf{k}) = 2[\hat{K}(\mathbf{0}) - \hat{K}(\mathbf{k})]$. We assume a simple ferromagnetic nearest-neighbor interaction

$$\delta \hat{K}(\mathbf{k}) = \frac{2}{\tilde{a}^2} \sum_{\alpha=1}^d [1 - \cos(\tilde{a} k_\alpha)], \quad (2.19)$$

which has the isotropic long-wavelength form

$$\delta \hat{K}(\mathbf{k}) = \mathbf{k}^2 + O(k^4). \quad (2.20)$$

Thus, it is appropriate to define a single second-moment bulk correlation length ξ^\pm above (+) and below (−) T_c [see, e.g., Eq. (3.4) of [7]]. As a reference length that is finite for both $n = 1$ and ∞ , we shall use the asymptotic amplitude ξ_{0+} of the second-moment bulk correlation length above T_c ,

$$\xi^+ = \xi_{0+} t^{-\nu}. \quad (2.21)$$

For small $|t|$, the asymptotic bulk power law is $f_{b,s}(t) = A^\pm |t|^{d\nu}$. Due to two-scale factor universality for isotropic systems [7], this can be written as

$$f_{b,s}(t) = \begin{cases} Q_1 (\xi_{0+}^{-1} t^\nu)^d & \text{for } T > T_c, \\ (A^-/A^+) Q_1 (\xi_{0+}^{-1} |t|^\nu)^d & \text{for } T < T_c, \end{cases} \quad (2.22)$$

with a universal constant Q_1 and the universal ratio of the specific-heat amplitudes A^-/A^+ .

The finite-size scaling form of the singular part of the free energy density is, for isotropic systems in the asymptotic critical region $|t| \ll 1$, $L/\tilde{a} \gg 1$, $L_\parallel/\tilde{a} \gg 1$ [7,37],

$$f_s(t, L, L_\parallel) = L^{-d} F(\tilde{x}, \rho), \quad (2.23)$$

where $F(\tilde{x}, \rho)$ is a dimensionless scaling function with the scaling variable

$$\tilde{x} = t(L/\xi_{0+})^{1/\nu}. \quad (2.24)$$

The bulk part $F_b^\pm(\tilde{x})$ of $F(\tilde{x}, \rho)$ is obtained from (2.22) and (2.23) in the limit of large $|\tilde{x}|$ as $L^d f_s(t, L, L_\parallel) \rightarrow F_b^\pm(\tilde{x})$ with

$$F_b^\pm(\tilde{x}) = \begin{cases} Q_1 \tilde{x}^{d\nu} & \text{for } T > T_c, \\ (A^-/A^+) Q_1 |\tilde{x}|^{d\nu} & \text{for } T < T_c. \end{cases} \quad (2.25)$$

This implies the scaling form

$$f_s^{ex}(t, L, L_\parallel) = L^{-d} F^{ex}(\tilde{x}, \rho), \quad (2.26)$$

$$F^{ex}(\tilde{x}, \rho) = F(\tilde{x}, \rho) - F_b^\pm(\tilde{x}). \quad (2.27)$$

Together with (2.15), this leads to the scaling form of the critical Casimir force for systems with isotropic interactions:

$$F_{\text{Casimir},s}(t, L, L_\parallel) = L^{-d} X(\tilde{x}, \rho) \quad (2.28)$$

with the scaling function

$$X(\tilde{x}, \rho) = (d-1) F^{ex}(\tilde{x}, \rho) - \frac{\tilde{x}}{\nu} \frac{\partial F^{ex}(\tilde{x}, \rho)}{\partial \tilde{x}} - \rho \frac{\partial F^{ex}(\tilde{x}, \rho)}{\partial \rho}. \quad (2.29)$$

These scaling functions have finite limits for $\rho \rightarrow 0$ at fixed L and at fixed \tilde{x} corresponding to film geometry

$$f_{\text{film},s}(t, L) = L^{-d} F_{\text{film}}(\tilde{x}), \quad (2.30)$$

$$F_{\text{film}}(\tilde{x}) = \lim_{\rho \rightarrow 0} F(\tilde{x}, \rho), \quad (2.31)$$

$$F_{\text{film}}^{ex}(\tilde{x}) = \lim_{\rho \rightarrow 0} F^{ex}(\tilde{x}, \rho), \quad (2.32)$$

$$X_{\text{film}}(\tilde{x}) = \lim_{\rho \rightarrow 0} X(\tilde{x}, \rho) = (d-1)F_{\text{film}}^{ex}(\tilde{x}) - \frac{\tilde{x}}{\nu} \frac{\partial F_{\text{film}}^{ex}(\tilde{x})}{\partial \tilde{x}}. \quad (2.33)$$

Note that ν denotes the *bulk* critical exponent and \tilde{x} is the scaling variable with respect to *bulk* criticality, not with respect to film criticality.

In a rod-shaped geometry with $\rho \gg 1$, a representation of the scaling form in terms of the length L_{\parallel} and of the scaling variable

$$\tilde{x}_{\parallel} = t(L_{\parallel}/\xi_{0+})^{1/\nu}, \quad (2.34)$$

rather than in terms of \tilde{x} , is more appropriate. Because of

$$\tilde{x} = \tilde{x}_{\parallel} \rho^{1/\nu}, \quad (2.35)$$

we obtain from (2.15), (2.23), (2.24), (2.26), and (2.27)

$$f_s(t, L, L_{\parallel}) = L_{\parallel}^{-d} \Phi(\tilde{x}_{\parallel}, \rho), \quad (2.36)$$

$$f_s^{ex}(t, L, L_{\parallel}) = L_{\parallel}^{-d} \Phi^{ex}(\tilde{x}_{\parallel}, \rho), \quad (2.37)$$

$$F_{\text{Casimir},s}(t, L, L_{\parallel}) = L_{\parallel}^{-d} \Xi(\tilde{x}_{\parallel}, \rho), \quad (2.38)$$

with the scaling functions

$$\Phi(\tilde{x}_{\parallel}, \rho) = \rho^{-d} F(\tilde{x}_{\parallel} \rho^{1/\nu}, \rho), \quad (2.39)$$

$$\Phi^{ex}(\tilde{x}_{\parallel}, \rho) = \rho^{-d} F^{ex}(\tilde{x}_{\parallel} \rho^{1/\nu}, \rho), \quad (2.40)$$

$$\begin{aligned} \Xi(\tilde{x}_{\parallel}, \rho) &= \rho^{-d} X(\tilde{x}_{\parallel} \rho^{1/\nu}, \rho) \\ &= -\Phi^{ex}(\tilde{x}_{\parallel}, \rho) + (1/\rho) \frac{\partial \Phi^{ex}(\tilde{x}_{\parallel}, \rho)}{\partial (1/\rho)}. \end{aligned} \quad (2.41)$$

It turns out that they have finite limits for $\rho \rightarrow \infty$ at fixed L_{\parallel} and fixed \tilde{x}_{\parallel} corresponding to cylinder geometry

$$f_{\text{cyl},s}(t, L_{\parallel}) = L_{\parallel}^{-d} \Phi_{\text{cyl}}(\tilde{x}_{\parallel}), \quad (2.42)$$

$$\Phi_{\text{cyl}}(\tilde{x}_{\parallel}) = \lim_{\rho \rightarrow \infty} \Phi(\tilde{x}_{\parallel}, \rho), \quad (2.43)$$

$$\Phi_{\text{cyl}}^{ex}(\tilde{x}_{\parallel}) = \lim_{\rho \rightarrow \infty} \Phi^{ex}(\tilde{x}_{\parallel}, \rho), \quad (2.44)$$

$$\Xi_{\text{cyl}}(\tilde{x}_{\parallel}) = \lim_{\rho \rightarrow \infty} \Xi(\tilde{x}_{\parallel}, \rho) = -\Phi_{\text{cyl}}^{ex}(\tilde{x}_{\parallel}). \quad (2.45)$$

Quantitative results for the various scaling functions will be presented in Sec. III for $n = \infty$ and in Secs. V and VI for $n = 1$.

We recall that all finite-size scaling forms given in this and in the subsequent sections are not valid in a small part of the asymptotic region for large L (or large L_{\parallel}) at fixed $t \neq 0$ in the $L^{1/\nu}$ - t plane (or $L_{\parallel}^{1/\nu}$ - t plane) above and below T_c (corresponding to the shaded regions in Fig. 2) where exponential nonscaling terms exist that depend explicitly on the lattice constant \tilde{a} . This issue will be discussed in Sec. VI.

III. LARGE- n LIMIT

A. Free energy density

By generalizing Eq. (6.30) of Ref. [7] to $L_{\parallel}^{d-1} \times L$ geometry, we obtain, for the free energy density per component

in the limit $n \rightarrow \infty$ at fixed u_{0n} ,

$$\begin{aligned} f(t, L, L_{\parallel}) &= \lim_{n \rightarrow \infty} [-(nV)^{-1} \ln Z(t, L, L_{\parallel})] \\ &= -\frac{\ln(2\pi)}{2\tilde{a}^d} - \frac{(r_0 - \chi^{-1})^2}{16u_{0n}} \\ &\quad + \frac{1}{2V} \sum_{\mathbf{k}} \ln\{\chi^{-1} + \delta\hat{K}(\mathbf{k})\tilde{a}^2\}, \end{aligned} \quad (3.1)$$

where $Z(t, L, L_{\parallel})$ is defined by (2.5) and $\chi(t, L, L_{\parallel})^{-1}$ is determined implicitly by

$$\chi^{-1} = r_0 + \frac{4u_{0n}}{V} \sum_{\mathbf{k}} [\chi^{-1} + \delta\hat{K}(\mathbf{k})]^{-1}. \quad (3.2)$$

The condition $\chi^{-1} = 0$ for bulk ($L \rightarrow \infty$, $L_{\parallel} \rightarrow \infty$) criticality yields the critical value of r_0 as

$$r_{0c} = -4u_{0n} \int_{\mathbf{k}} \delta\hat{K}(\mathbf{k})^{-1}, \quad \int_{\mathbf{k}} \equiv \prod_{\alpha=1}^d \int_{-\pi/\tilde{a}}^{\pi/\tilde{a}} \frac{dk_{\alpha}}{2\pi}. \quad (3.3)$$

Equations (3.1) and (3.2) are valid for $T \geq T_c$ ($r_0 \geq r_{0c}$) and $T < T_c$ ($r_0 < r_{0c}$). For $T \geq T_c$, the quantity $\chi(t, L, L_{\parallel})$ represents the susceptibility per component.

B. Exact scaling functions

In the following, we present exact results for the finite-size scaling functions F , Φ , F^{ex} , Φ^{ex} , X , and Ξ in $2 < d < 4$ dimensions. We rewrite (3.1) and (3.2) in terms of $r_0 - r_{0c} = a_0 t$ and assume large L/\tilde{a} , large L_{\parallel}/\tilde{a} , small $|r_0 - r_{0c}|\tilde{a}^2 \ll 1$, and $|r_0 - r_{0c}|L^2 \lesssim O(1)$, $|r_0 - r_{0c}|L_{\parallel}^2 \lesssim O(1)$. Evaluation of the sums in (3.1) and (3.2) (see the Appendix) leads to the scaling form of $f_s(t, L, L_{\parallel})$ [Eqs. (2.23) and (2.24)], where $\nu = (d-2)^{-1}$ and

$$\xi_{0+} = \left(\frac{4u_{0n}A_d}{\varepsilon a_0} \right)^{1/(d-2)} \quad (3.4)$$

with the geometric factor

$$A_d = \frac{\Gamma(3-d/2)}{2^{d-2}\pi^{d/2}(d-2)}. \quad (3.5)$$

For an arbitrary finite shape factor $0 < \rho < \infty$, we find the finite-size scaling function

$$F(\tilde{x}, \rho) = \frac{A_d}{2\varepsilon} \left[\tilde{x} P(\tilde{x}, \rho)^2 - \frac{2}{d} P(\tilde{x}, \rho)^d \right] + \frac{1}{2} \mathcal{G}_0[P(\tilde{x}, \rho)^2, \rho], \quad (3.6)$$

$$\begin{aligned} \mathcal{G}_j(P^2, \rho) &= (4\pi^2)^{-j} \int_0^\infty dz z^{j-1} \exp\left(-\frac{P^2 z}{4\pi^2}\right) \\ &\quad \times \{(\pi/z)^{d/2} - [\rho K(\rho^2 z)]^{d-1} K(z)\}, \end{aligned} \quad (3.7)$$

where $P(\tilde{x}, \rho)$ is determined implicitly by

$$P^{d-2} = \tilde{x} - \frac{\varepsilon}{A_d} \mathcal{G}_1(P^2, \rho) \quad (3.8)$$

with

$$K(z) = \sum_{m=-\infty}^{\infty} \exp(-zm^2). \quad (3.9)$$

The earlier result of Eqs. (6.32)–(6.34) of [7] for cubic geometry is obtained from Eqs. (3.6)–(3.8) by setting $\rho = 1$.

In the film limit $\rho \rightarrow 0$ at finite L , we obtain $\rho K(\rho^2 z) \rightarrow (\pi/z)^{1/2}$,

$$F_{\text{film}}(\tilde{x}) = \frac{A_d}{2\varepsilon} \left[\tilde{x} P(\tilde{x})^2 - \frac{2}{d} P(\tilde{x})^d \right] + \frac{1}{2} \mathcal{G}_{0,\text{film}}[P(\tilde{x})^2], \quad (3.10)$$

$$\mathcal{G}_{j,\text{film}}(P^2) = (4\pi^2)^{-j} \int_0^\infty dz z^{j-1} \exp\left(-\frac{P^2 z}{4\pi^2}\right) \left(\frac{\pi}{z}\right)^{(d-1)/2} \times \{(\pi/z)^{1/2} - K(z)\}, \quad (3.11)$$

where $P(\tilde{x})$ is determined implicitly by

$$P^{d-2} = \tilde{x} - \frac{\varepsilon}{A_d} \mathcal{G}_{1,\text{film}}(P^2). \quad (3.12)$$

For $n \rightarrow \infty$, a finite film-critical temperature $0 < T_{c,\text{film}}(L) < T_c$ exists only in $d > 3$ dimensions, whereas $T_{c,\text{film}}(L) = 0$ in $d \leq 3$ dimensions. Equations (3.10)–(3.12) are valid in the asymptotic region near bulk T_c .

In the cylinder limit $\rho \rightarrow \infty$ at finite L_\parallel , we obtain $K(\rho^2 z) \rightarrow 1$, $P(\tilde{x}, \rho)/\rho \rightarrow P_{\text{cyl}}(\tilde{x}_\parallel)$,

$$\Phi_{\text{cyl}}(\tilde{x}_\parallel) = \frac{A_d}{2\varepsilon} \left[\tilde{x}_\parallel P_{\text{cyl}}(\tilde{x}_\parallel)^2 - \frac{2}{d} P_{\text{cyl}}(\tilde{x}_\parallel)^d \right] + \frac{1}{2} \mathcal{G}_{0,\text{cyl}}[P_{\text{cyl}}(\tilde{x}_\parallel)^2], \quad (3.13)$$

$$\mathcal{G}_{j,\text{cyl}}(P_{\text{cyl}}^2) = (4\pi^2)^{-j} \int_0^\infty dz z^{j-1} \exp\left(-\frac{z P_{\text{cyl}}^2}{4\pi^2}\right) (\pi/z)^{1/2} \times \{(\pi/z)^{(d-1)/2} - [K(z)]^{d-1}\}, \quad (3.14)$$

where $P_{\text{cyl}}(\tilde{x}_\parallel)$ is determined implicitly by

$$P_{\text{cyl}}^{d-2} = \tilde{x}_\parallel - \frac{\varepsilon}{A_d} \mathcal{G}_{1,\text{cyl}}(P_{\text{cyl}}^2). \quad (3.15)$$

In this cylinder limit, the system has an infinite extension only in the d th direction, i.e., it is essentially one dimensional, thus, no finite critical temperature exists in the cylinder case at finite L_\parallel . Equations (3.13)–(3.15) are valid in the asymptotic region near bulk T_c .

The bulk part $F_b^\pm(\tilde{x})$ of $F(\tilde{x}, \rho)$ in the large- n limit is given by (2.25) with $Q_1 = (d-2)A_d/[2d(4-d)]$ and $A^-/A^+ = 0$. Correspondingly, the bulk part of $\Phi(\tilde{x}_\parallel, \rho)$ is $\Phi_b^\pm(\tilde{x}_\parallel) = F_b^\pm(\tilde{x}_\parallel)$. From (2.27) and (2.40), we then obtain the scaling functions F^{ex} and Φ^{ex} of the excess free energy density.

The scaling functions X and Ξ of the Casimir force are obtained from F^{ex} and Φ^{ex} according to (2.29), (2.33), (2.41), and (2.45). All scaling functions are shown in Figs. 3 and 4 for several values of ρ in three dimensions, illustrating the crossover from film geometry ($\rho = 0$, dotted lines in Fig. 3) over cubic geometry (double-dotted-dashed lines) to cylinder geometry ($1/\rho = 0$, dotted lines in Fig. 4). We see that, for $O(-10) < \tilde{x} \leq \infty$ and $O(-10) < \tilde{x}_\parallel \leq \infty$, the scaling functions for slab ($\rho < 1$) and rod ($1/\rho < 1$) geometries, respectively, provide a reasonable approximation for the scaling functions (i) for film geometry if the shape factor ρ is sufficiently small, and (ii) for cylinder geometry if the inverse shape factor $1/\rho$ is sufficiently small. This is not true, however, in the low-temperature limit $\tilde{x} \rightarrow -\infty$ and $\tilde{x}_\parallel \rightarrow -\infty$, respectively (see the following section).

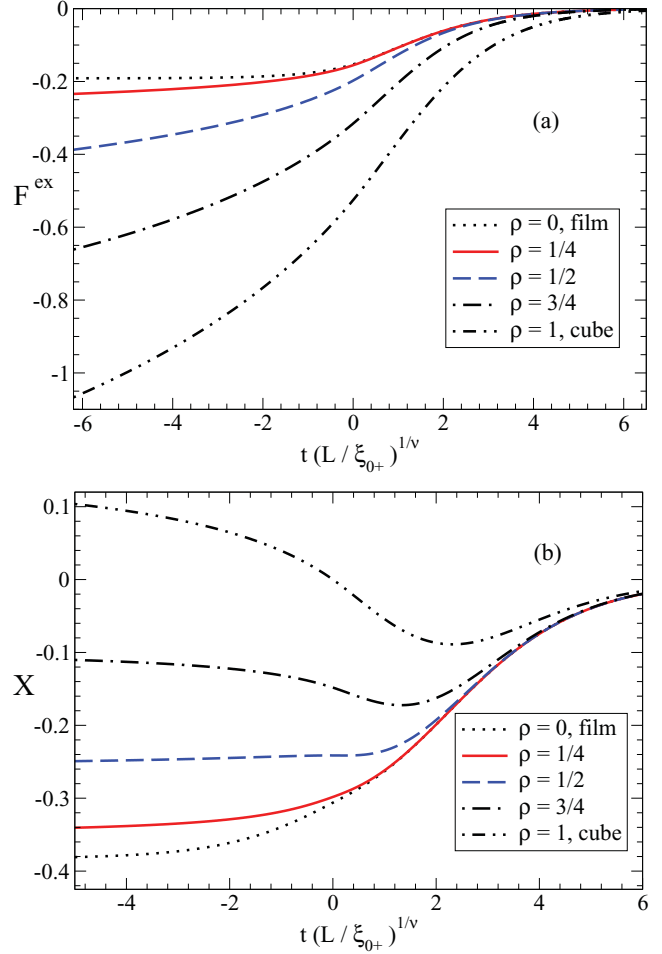


FIG. 3. (Color online) Scaling functions (a) $F^{\text{ex}}(\tilde{x}, \rho)$ [Eqs. (2.27) and (3.6)–(3.8)] and (b) $X(\tilde{x}, \rho)$ [Eq. (2.29)] as a function of $\tilde{x} = t(L/\xi_{0+})^{1/\nu}$ in the large- n limit in three dimensions for film geometry ($\rho = 0$, dotted lines), for slab geometry (solid lines: $\rho = 1/4$, dashed lines: $\rho = 1/2$, dotted-dashed lines: $\rho = 3/4$), and for cubic geometry ($\rho = 1$, double-dotted-dashed lines). For $\tilde{x} \rightarrow -\infty$, the curves in (a) with $\rho > 0$ diverge logarithmically toward $-\infty$, whereas the $\rho = 0$ curve in (a) has a finite low-temperature limit -0.191 . All curves in (b) have finite limits for $\tilde{x} \rightarrow -\infty$ as given by (3.21) and (3.23).

C. Monotonicity properties at fixed ρ

For fixed ρ , $F^{\text{ex}}(\tilde{x}, \rho)$ and $\Phi^{\text{ex}}(\tilde{x}_\parallel, \rho)$ are monotonically increasing functions of \tilde{x} and \tilde{x}_\parallel , respectively [see Figs. 3(a) and 4(a)]. They vanish exponentially fast for $\tilde{x} \rightarrow \infty$ and $\tilde{x}_\parallel \rightarrow \infty$ and have logarithmic divergencies toward $-\infty$ for $\tilde{x} \rightarrow -\infty$ and $\tilde{x}_\parallel \rightarrow -\infty$, respectively, for finite $0 < \rho < \infty$.

To derive the latter property, consider the quantity P as determined by (3.8). It is finite and positive for $-\infty < \tilde{x} < \infty$ and vanishes for $\tilde{x} \rightarrow -\infty$. More specifically, the function \mathcal{G}_1 has the divergent small- P^2 behavior $\mathcal{G}_1(P^2, \rho) \approx -\rho^{d-1} P^{-2}$ [see (A8) in the Appendix]. According to (3.8), this implies that P^2 vanishes as $P^2 \approx \varepsilon A_d^{-1} \rho^{d-1} (-\tilde{x})^{-1}$ for $\tilde{x} \rightarrow -\infty$. Thus, the behavior of $F(\tilde{x}, \rho)$ [Eq. (3.6)] for large negative \tilde{x} is given by

$$F(\tilde{x}, \rho) = F^{\text{ex}}(\tilde{x}, \rho) \approx -\frac{1}{2} \rho^{d-1} + \frac{1}{2} \mathcal{G}_0[P(\tilde{x}, \rho)^2, \rho] \quad (3.16)$$

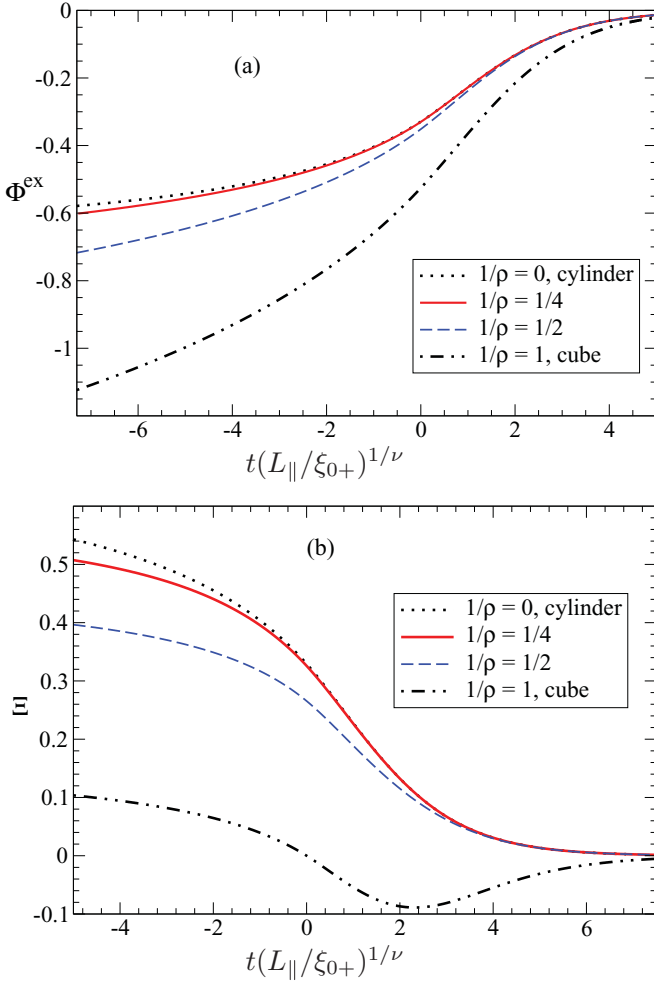


FIG. 4. (Color online) Scaling functions (a) $\Phi^{ex}(\tilde{x}_{||}, \rho)$ [Eq. (2.40)] and (b) $\Xi(\tilde{x}_{||}, \rho)$ [Eq. (2.41)] as a function of $\tilde{x}_{||} = t(L_{||}/\xi_{0+})^{1/\nu}$ in the large- n limit in three dimensions for cylinder geometry ($1/\rho = 0$, dotted lines), for rod geometry (solid lines: $1/\rho = 1/4$, dashed lines: $1/\rho = 1/2$), and for cubic geometry ($1/\rho = 1$, double-dotted-dashed lines). For $\tilde{x}_{||} \rightarrow -\infty$, the curves in (a) with $1/\rho > 0$ diverge logarithmically toward $-\infty$, whereas the $1/\rho = 0$ curve in (a) has a finite low-temperature limit -0.719 . All curves in (b) have finite limits for $\tilde{x}_{||} \rightarrow -\infty$ as given by (3.22) and (3.24).

for $-\tilde{x} \gg 1$. The function \mathcal{G}_0 has a divergent small- P^2 behavior as given by (A4) in the Appendix. The resulting logarithmic divergency is

$$F^{ex}(\tilde{x}, \rho) \approx -\frac{1}{2}\rho^{d-1} \ln\left(\frac{4\pi^2 A_d |\tilde{x}|}{\varepsilon \rho^{d-1}}\right) - \frac{1}{2}\rho^{d-1} + \frac{1}{2}\mathcal{C}_0(\rho) \quad (3.17)$$

with $\mathcal{C}_0(\rho)$ given by (A6). For finite $0 < \rho < \infty$, Eqs. (2.35) and (2.40) imply a corresponding logarithmic divergency of $\Phi^{ex}(\tilde{x}_{||}, \rho)$ for $\tilde{x}_{||} \rightarrow -\infty$.

By contrast, we shall find a *nonmonotonic* dependence of the scaling functions F^{ex} and Φ^{ex} on \tilde{x} and $\tilde{x}_{||}$ for the $n = 1$ universality class for finite $0 < \rho < \infty$ in the central finite-size scaling regime described in Sec. V below.

For the film system in the large- n limit, we confine ourselves to the case $d = 3$. We find from (3.11) that $\mathcal{G}_{1,\text{film}}(P^2) \approx$

$(4\pi)^{-1} \ln P^2$ for small P^2 and that P^2 vanishes as $P^2 \propto e^{\tilde{x}}$ for $\tilde{x} \rightarrow -\infty$. This implies that $F_{\text{film}}^{ex}(\tilde{x})$ has a *finite* value in the low-temperature limit [40] [compare Fig. 3(a)]

$$\lim_{\tilde{x} \rightarrow -\infty} F_{\text{film}}^{ex}(\tilde{x}) = \frac{1}{2}\mathcal{G}_{0,\text{film}}(0) = -0.191 \quad \text{for } d = 3. \quad (3.18)$$

In the cylinder system in the large- n limit, we find from (3.14) that $\mathcal{G}_{1,\text{cyl}}(P_{\text{cyl}}^2) \approx -c_1 P_{\text{cyl}}^{-1}$ for small P_{cyl} with $c_1 = (4\pi)^{-1/2} \int_0^\infty dy y^{-1/2} e^{-y} > 0$ and $P_{\text{cyl}} \approx c_1 \varepsilon A_d^{-1} (-\tilde{x}_{||})^{-1}$ for $\tilde{x}_{||} \rightarrow -\infty$. This implies that, for $2 < d < 4$, $\Phi_{\text{cyl}}^{ex}(\tilde{x}_{||})$ has a *finite* value in the low-temperature limit

$$\lim_{\tilde{x}_{||} \rightarrow -\infty} \Phi_{\text{cyl}}^{ex}(\tilde{x}_{||}) = \frac{1}{2} \mathcal{G}_{0,\text{cyl}}(0) \quad (3.19)$$

with $\frac{1}{2} \mathcal{G}_{0,\text{cyl}}(0) = -0.719$ for $d = 3$ [compare Fig. 4(a)].

In contrast to F^{ex} and Φ^{ex} , the scaling functions X and Ξ turn out to be *nonmonotonic* functions of their scaling variables \tilde{x} and $\tilde{x}_{||}$, respectively, in an intermediate range of ρ where $\rho \sim O(1)$ [see Figs. 3(b) and 4(b)]. In this range, X exhibits a change of sign near $\tilde{x} = 0$: The Casimir force changes from a repulsive force below T_c to an attractive force above T_c . Especially for $\rho = 1$, $d = 3$, this change of sign occurs exactly at T_c where $X(0, 1) = 0$, $\Xi(0, 1) = 0$. In the range $\rho \lesssim 1/2$, $X < 0$ is a monotonically increasing function of \tilde{x} . In the range $\rho \gtrsim 3/2$, $\Xi > 0$ is a monotonically decreasing function of $\tilde{x}_{||}$.

Above T_c , X and Ξ have an exponential decay toward zero as functions of $\tilde{x} \gg 1$ and $\tilde{x}_{||} \gg 1$, respectively, as follows from the exponential decay of F^{ex} and Φ^{ex} . Below T_c , the scaling functions X and Ξ have *finite* values in the low-temperature limits $\tilde{x} \rightarrow -\infty$ and $\tilde{x}_{||} \rightarrow -\infty$, respectively, for all $-\infty \leq \rho \leq \infty$, unlike the divergent behavior of F^{ex} and Φ^{ex} for finite ρ . To derive the low-temperature limit of X , we use Eqs. (2.27) and (3.6) to rewrite (2.29) as

$$X(\tilde{x}, \rho) = F_b^\pm(\tilde{x}) + \frac{A_d}{\varepsilon} \left[\frac{1}{2} \tilde{x} P^2 - \frac{d-1}{d} P^d \right] + \frac{1}{2} \left[(d-1) \mathcal{G}_0(P^2, \rho) - \rho \frac{\partial \mathcal{G}_0(P^2, \rho)}{\partial \rho} \right] \quad (3.20)$$

with $P(\tilde{x}, \rho)^2$ determined by (3.8). For $P^2 \rightarrow 0$, the divergent parts of the last two terms cancel each other, which leads to a finite limit

$$\lim_{\tilde{x} \rightarrow -\infty} X(\tilde{x}, \rho) = -\frac{1}{2}\rho^{d-1} + \frac{1}{2} \lim_{P \rightarrow 0} \left[(d-1) \mathcal{G}_0(P^2, \rho) - \rho \frac{\partial \mathcal{G}_0(P^2, \rho)}{\partial \rho} \right] \quad (3.21)$$

with a nontrivial ρ dependence. Similarly, we obtain a finite limit

$$\lim_{\tilde{x}_{||} \rightarrow -\infty} \Xi(\tilde{x}_{||}, \rho) = \rho^{-d} \lim_{\tilde{x} \rightarrow -\infty} X(\tilde{x}, \rho). \quad (3.22)$$

This is in contrast to the exponential decay of X and Ξ toward zero for $\tilde{x} \rightarrow -\infty$ and $\tilde{x}_{||} \rightarrow -\infty$, respectively, for the $n = 1$ universality class that we shall find in Sec. VI below.

For film and cylinder geometries in the large- n limit, the low-temperature limits are

$$\lim_{\tilde{x} \rightarrow -\infty} X_{\text{film}}(\tilde{x}) = 2F_{\text{film}}^{ex}(-\infty) = \mathcal{G}_{0,\text{film}}(0) = -0.383 \quad (3.23)$$

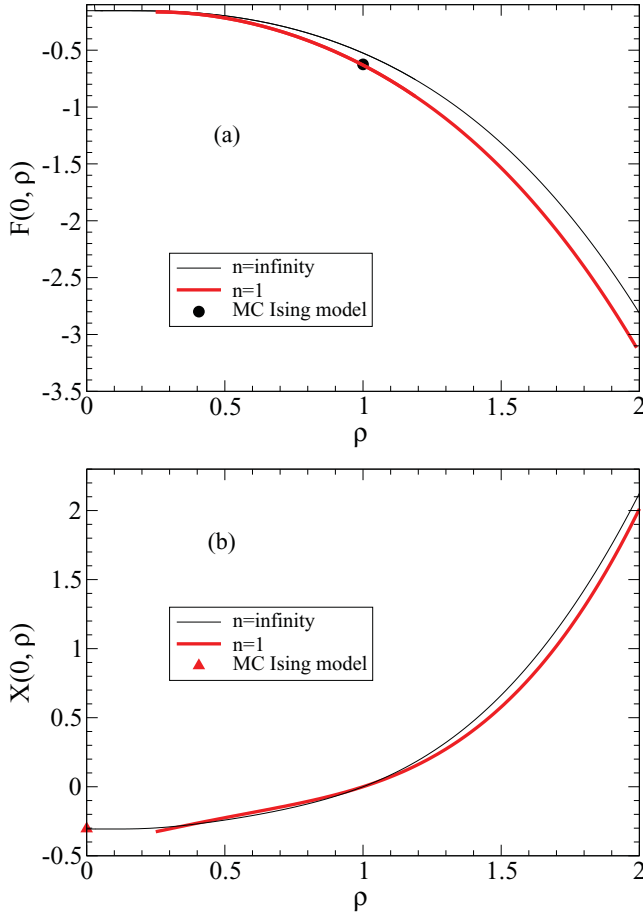


FIG. 5. (Color online) Critical amplitudes (a) $F(0, \rho)$ [Eq. (2.27)] and (b) $X(0, \rho)$ [Eq. (5.10)] at T_c in three dimensions as a function of the aspect ratio ρ in the large- n limit [thin lines, from (3.6)] and for $n = 1$ [thick lines, from (5.1)]. For $n = \infty$, $F_{\text{film}}(0) \equiv F(0, 0) = -0.153$ and $X_{\text{film}}(0) \equiv X(0, 0) = 2F_{\text{film}}(0) = -0.306$. At $\rho = 1$, $X(0, 1)$ vanishes for both $n = \infty$ and 1. Monte Carlo data of the $d = 3$ Ising model for $\rho = 1$ by Mon [41] [full circle in (a)] and for $\rho = 0$ by Vasilyev *et al.* [16] [triangle in (b)]. See also Fig. 7.

for $d = 3$ [see Fig. 3(b)], in agreement with the earlier result for the spherical model [22,40], and

$$\lim_{\tilde{x}_{\parallel} \rightarrow -\infty} \Xi_{\text{cyl}}(\tilde{x}_{\parallel}) = -\Phi_{\text{cyl}}(-\infty) = -\frac{1}{2} \mathcal{G}_{0, \text{cyl}}(0) \quad (3.24)$$

for $2 < d < 4$, with $-\frac{1}{2} \mathcal{G}_{0, \text{cyl}}(0) = 0.719$ for $d = 3$ [see Fig. 4(b)].

D. Monotonicity properties at fixed temperature

From Figs. 3 and 4, we also infer monotonicity properties at fixed \tilde{x} and \tilde{x}_{\parallel} , respectively, i.e., at fixed temperature. For fixed \tilde{x} , $F^{ex}(\tilde{x}, \rho)$ is monotonically decreasing with increasing ρ , whereas $X(\tilde{x}, \rho)$ is monotonically increasing with increasing ρ . For fixed \tilde{x}_{\parallel} , both $\Phi^{ex}(\tilde{x}_{\parallel}, \rho)$ and $\Xi^{ex}(\tilde{x}_{\parallel}, \rho)$ are monotonically decreasing with increasing $1/\rho$. This monotonicity is demonstrated by the thin lines in Figs. 5 and 6 at bulk T_c ($\tilde{x} = 0$, $\tilde{x}_{\parallel} = 0$). These lines also exhibit a monotonic change of the curvature toward zero for $\rho \rightarrow 0$ and for $1/\rho \rightarrow 0$, respectively. For comparison, corresponding curves are also shown for the $n = 1$ universality class (thick lines in Figs. 5

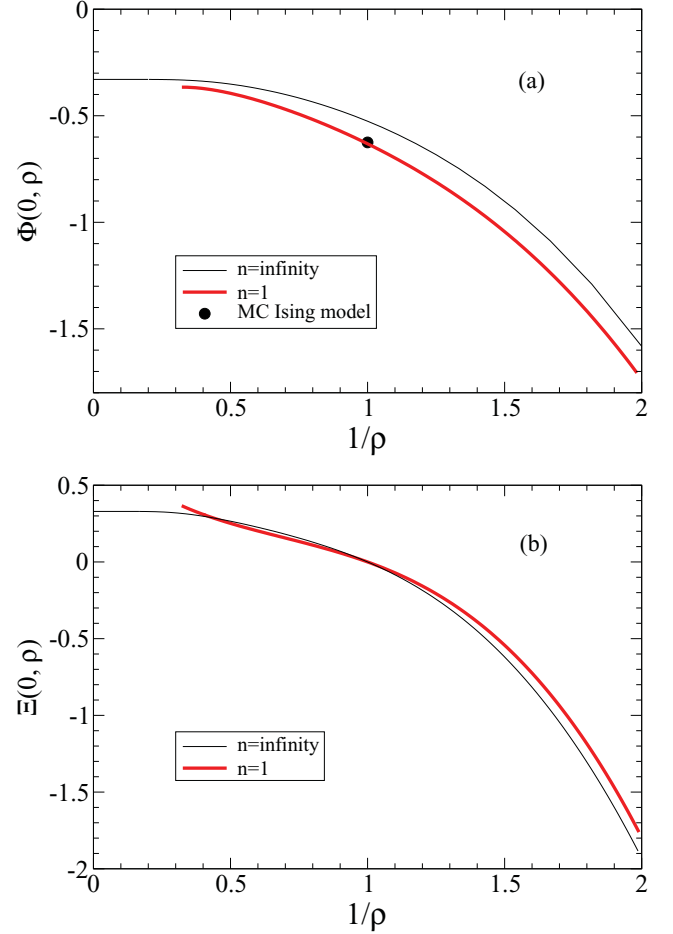


FIG. 6. (Color online) Critical amplitudes (a) $\Phi(0, \rho)$ [Eq. (2.39)] and (b) $\Xi(0, \rho)$ [Eq. (5.11)] at T_c in three dimensions as a function of the inverse aspect ratio $1/\rho$ in the large- n limit [thin lines, from (3.6)] and for $n = 1$ [thick lines, from (5.1)]. For $n = \infty$, $\Phi_{\text{cyl}}(0) \equiv \Phi(0, \infty) = -0.329 = -\Xi_{\text{cyl}}(0) = -\Xi(0, \infty)$. At $1/\rho = 1$, $\Xi(0, 1)$ vanishes for both $n = \infty$ and 1. Monte Carlo data of the $d = 3$ Ising model for $\rho = 1$ by Mon [41] [full circle in (a)]. See also Fig. 8.

and 6) that will be derived in the subsequent sections. On the basis of these results, we are led to our hypothesis that the monotonicity properties mentioned above are valid not only for $n = \infty$ but are general features of the free energy and the Casimir force (for periodic BC) that are valid for all n in the whole range $1 \leq n \leq \infty$.

IV. PERTURBATION THEORY FOR $n = 1$ IN THE CENTRAL FINITE-SIZE REGIME

In this and the subsequent sections, we confine ourselves to the case of a one-component order parameter.

A. Perturbation approach for the free energy density

The basic ingredients of our perturbation approach for $L_{\parallel}^{d-1} \times L$ geometry are similar to those developed previously for cubic geometry [7]. The starting point is a decomposition of the variables $\varphi_j = \Phi + \sigma_j$ into the lowest (homogeneous)

mode amplitude Φ and higher-mode contributions σ_j ,

$$\Phi = V^{-1} \hat{\phi}(\mathbf{0}) = N^{-1} \sum_j \varphi_j, \quad (4.1)$$

$$\sigma_j = \frac{1}{V} \sum_{\mathbf{k} \neq \mathbf{0}} e^{i\mathbf{k} \cdot \mathbf{x}_j} \hat{\phi}(\mathbf{k}). \quad (4.2)$$

Correspondingly, the Hamiltonian H and the partition function Z are decomposed as

$$H = H_0 + \tilde{H}(\Phi, \sigma), \quad (4.3)$$

$$H_0(r_0, u_0, V, \Phi^2) = V \left(\frac{1}{2} r_0 \Phi^2 + u_0 \Phi^4 \right), \quad (4.4)$$

$$\begin{aligned} \tilde{H}(\Phi, \sigma) = & \tilde{a}^d \left\{ \sum_{j=1}^N \left[\left(\frac{r_0}{2} + 6u_0 \Phi^2 \right) \sigma_j^2 + 4u_0 \Phi \sigma_j^3 + u_0 \sigma_j^4 \right] \right. \\ & \left. + \sum_{i,j=1}^N \frac{K_{i,j}}{2} (\sigma_i - \sigma_j)^2 \right\}, \end{aligned} \quad (4.5)$$

$$Z = \frac{V^{1/2}}{\tilde{a}} \int_{-\infty}^{\infty} d\Phi \exp\{-[H_0 + \tilde{\Gamma}(\Phi^2)]\}, \quad (4.6)$$

$$\tilde{\Gamma}(\Phi^2) = -\ln \left[\prod_{\mathbf{k}' \neq \mathbf{0}} \frac{1}{\tilde{a} V^{1/2}} \int d\hat{\sigma}(\mathbf{k}) \right] \exp[-\tilde{H}(\Phi, \sigma)], \quad (4.7)$$

where $\hat{\sigma}(\mathbf{k}) \equiv \hat{\phi}(\mathbf{k})$ for $\mathbf{k} \neq \mathbf{0}$. We shall calculate the partition function and the free energy by first determining $\tilde{\Gamma}(\Phi^2)$ by means of perturbation theory at given Φ and subsequently performing the integration over Φ . Since $\exp[-\tilde{\Gamma}(\Phi^2)]$ is proportional to the order-parameter distribution function, which is a physical quantity in its own right, we shall maintain the exponential form of $\exp[-\tilde{\Gamma}(\Phi^2)]$ without further expansion.

The decompositions (4.3)–(4.7) and the perturbative treatment of the higher modes are reasonable as long as there exists a single lowest mode that is well separated from the higher modes. This is, of course, not the case in the film limit $\rho \rightarrow 0$ and in the cylinder limit $\rho \rightarrow \infty$, where the system has a lowest-mode *continuum* and where a revised perturbation approach would be necessary. In Sec. V below, a quantitative estimate will be given as to in which range of $0 < \rho < \infty$ our perturbation approach is expected to be applicable.

Since the details of the perturbation approach for $f(t, L, L_{\parallel})$ are parallel to those presented in [7] for cubic geometry, we directly turn to the result. Our perturbation expression for the bare free energy density reads as

$$\begin{aligned} f = & -\frac{N-1}{2V} \ln(2\pi) + \frac{1}{2} S_0(r_{0L}, L, \rho) \\ & -\frac{1}{V} \ln \int_{-\infty}^{\infty} ds \exp\left(-\frac{1}{2} y_0^{\text{eff}} s^2 - s^4\right) \\ & -\frac{1}{2V} \ln \left[\frac{V^{1/2} w_0^{\text{eff}}}{\tilde{a}^2} \right] - 6u_0 M_0^2 S_1(r_{0L}, L, \rho) \\ & - 36u_0^2 M_0^4 S_2(r_{0L}, L, \rho) \end{aligned} \quad (4.8)$$

with

$$\begin{aligned} y_0^{\text{eff}} = & V^{1/2} u_0^{-1/2} \{ r_0 [1 + 18u_0 S_2(r_{0L}, L, \rho)] \\ & + 12u_0 S_1(r_{0L}, L, \rho) + 144u_0^2 M_0^2 S_2(r_{0L}, L, \rho) \}, \end{aligned} \quad (4.9)$$

$$w_0^{\text{eff}} = u_0^{-1/2} [1 + 18u_0 S_2(r_{0L}, L, \rho)]. \quad (4.10)$$

Here, $S_i(r_{0L}, L, \rho)$ denote the sums over the higher modes

$$S_0(r_{0L}, L, \rho) = \frac{1}{V} \sum_{\mathbf{k} \neq \mathbf{0}} \ln\{[r_{0L} + \delta \hat{K}(\mathbf{k})] \tilde{a}^2\}, \quad (4.11)$$

$$S_m(r_{0L}, L, \rho) = \frac{1}{V} \sum_{\mathbf{k} \neq \mathbf{0}} \{[r_{0L} + \delta \hat{K}(\mathbf{k})]\}^{-m} \quad (4.12)$$

for $m = 1, 2$. The temperature dependence enters through the parameter

$$r_{0L}(r_0, u_0, V) = r_0 + 12u_0 M_0^2(r_0, u_0, V) \quad (4.13)$$

as well as through the lowest-mode average

$$M_0^2(r_0, u_0, V) = \frac{\int_{-\infty}^{\infty} d\Phi \Phi^2 \exp[-H_0(r_0, u_0, V)]}{\int_{-\infty}^{\infty} d\Phi \exp[-H_0(r_0, u_0, V)]}. \quad (4.14)$$

The positivity of $r_{0L} > 0$ for all r_0 permits us to apply the theory to the region below T_c . For finite V , M_0^2 and r_{0L} interpolate smoothly between the mean-field bulk limits above and below T_c :

$$\lim_{V \rightarrow \infty} M_0^2 \equiv M_{mf}^2 = \begin{cases} 0 & \text{for } r_0 \geq 0, \\ -r_0/(4u_0) & \text{for } r_0 \leq 0, \end{cases} \quad (4.15)$$

and

$$\lim_{V \rightarrow \infty} r_{0L} \equiv r_{mf} = \begin{cases} r_0 & \text{for } r_0 \geq 0, \\ -2r_0 & \text{for } r_0 \leq 0, \end{cases} \quad (4.16)$$

respectively. In the bulk limit, Eq. (4.8) correctly contains the bare bulk free energy density in one-loop order [i.e., up to $O(1)$]

$$f_b^+ = -\frac{\ln(2\pi)}{2\tilde{a}^d} + \frac{1}{2} \int_{\mathbf{k}} \ln\{[r_0 + \delta \hat{K}(\mathbf{k})] \tilde{a}^2\}, \quad (4.17)$$

$$\begin{aligned} f_b^- = & \frac{1}{2} r_0 M_{mf}^2 + u_0 M_{mf}^4 - \frac{\ln(2\pi)}{2\tilde{a}^d} \\ & + \frac{1}{2} \int_{\mathbf{k}} \ln\{[-2r_0 + \delta \hat{K}(\mathbf{k})] \tilde{a}^2\} \end{aligned} \quad (4.18)$$

above and below T_c , respectively. [For the symbol $\int_{\mathbf{k}}$, see Eq. (3.3).] In the derivation of (4.8), $\tilde{\Gamma}(\Phi^2)$ has been expanded around M_0^2 in powers of $\Phi^2 - M_0^2$ up to $O[(\Phi^2 - M_0^2)^2]$. Furthermore, an expansion with respect to u_0 at fixed r_{0L} has been made and has been truncated such that terms of $O(u_0^{3/2})$ are neglected. For a discussion of the order of the neglected terms, see [7,31,42].

B. Dependence on the aspect ratio ρ

Equations (4.8)–(4.10) are identical in structure with Eqs. (4.26)–(4.28) of [7], where a cubic geometry was considered. The new point of interest here is the dependence of the bare free energy density $f(t, L_{\parallel}, L)$ on the aspect ratio $\rho = L/L_{\parallel}$. The ρ dependence enters (i) through the volume

$$V = L_{\parallel}^{d-1} L = L^d \rho^{1-d}, \quad (4.19)$$

(ii) through the lowest-mode average

$$M_0^2(r_0, u_0, V) = (L^d \rho^{1-d} u_0)^{-1/2} \vartheta_2(y_0), \quad (4.20)$$

$$y_0 = r_0 (L^d \rho^{1-d} / u_0)^{1/2}, \quad (4.21)$$

$$\vartheta_2(y_0) = \frac{\int_0^\infty ds s^2 \exp(-\frac{1}{2} y_0 s^2 - s^4)}{\int_0^\infty ds \exp(-\frac{1}{2} y_0 s^2 - s^4)}, \quad (4.22)$$

and (iii) through the higher-mode sums $S_i(r_{0L}, L, \rho)$ [Eqs. (4.11) and (4.12)]. In the regime of large L/\tilde{a} , large L_\parallel/\tilde{a} , small $0 < (r_{0L})^{1/2} \tilde{a} \ll 1$, and fixed $0 < L(r_{0L})^{1/2} \lesssim O(1)$, $0 < L_\parallel(r_{0L})^{1/2} \lesssim O(1)$, these sums are evaluated for finite $0 < \rho < \infty$ in $2 < d < 4$ dimensions as (see Appendix B of [7] and our Appendix)

$$\begin{aligned} S_0(r_{0L}, L, \rho) &= \int_{\mathbf{k}} \ln\{\delta \hat{K}(\mathbf{k})\} \tilde{a}^2 + r_{0L} \int_{\mathbf{k}} [\delta \hat{K}(\mathbf{k})]^{-1} \\ &\quad - \frac{2A_d(r_{0L})^{d/2}}{d\varepsilon} + \frac{1}{L^d} \ln\left(\frac{L^2}{\tilde{a}^2 4\pi^2}\right) \\ &\quad + \frac{1 - \rho^{d-1}}{L^d} \ln(r_{0L} \tilde{a}^2) + \frac{1}{L^d} J_0(r_{0L} L^2, \rho), \end{aligned} \quad (4.23)$$

$$\begin{aligned} S_1(r_{0L}, L, \rho) &= \int_{\mathbf{k}} [\delta \hat{K}(\mathbf{k})]^{-1} - \frac{A_d}{\varepsilon} (r_{0L})^{(d-2)/2} \\ &\quad + \frac{1 - \rho^{d-1}}{L^d} (r_{0L})^{-1} + \frac{(L)^{2-d}}{(4\pi^2)} I_1(r_{0L} L^2, \rho), \end{aligned} \quad (4.24)$$

$$\begin{aligned} S_2(r_{0L}, L, \rho) &= \frac{A_d}{2\varepsilon} (d-2) (r_{0L})^{-\varepsilon/2} + \frac{1 - \rho^{d-1}}{L^d} (r_{0L})^{-2} \\ &\quad + \frac{(L)^{4-d}}{(4\pi^2)^2} I_2(r_{0L} L^2, \rho) \end{aligned} \quad (4.25)$$

with

$$\begin{aligned} J_0(x^2, \rho) &= \int_0^\infty dy y^{-1} \exp[-x^2 y / (4\pi^2)] \{(\pi/y)^{d/2} \\ &\quad - [\rho K(\rho^2 y)]^{d-1} K(y) + 1\} - e^{-y}, \end{aligned} \quad (4.26)$$

$$\begin{aligned} I_m(x^2, \rho) &= \int_0^\infty dy y^{m-1} \exp[-x^2 y / (4\pi^2)] \\ &\quad \times \{[\rho K(\rho^2 y)]^{d-1} K(y) - (\pi/y)^{d/2} - 1\} \end{aligned} \quad (4.27)$$

for $m = 1, 2$. [For $K(y)$, see Eq. (3.9).]

C. Bare perturbation result

It is appropriate to rewrite the free energy density f [Eq. (4.8)] in terms of $r_0 - r_{0c}$, where

$$r_{0c} = -12u_0 \int_{\mathbf{k}} [\delta \hat{K}(\mathbf{k})]^{-1} \quad (4.28)$$

is the critical value of r_0 up to $O(u_0)$. The resulting function is denoted as $\hat{f}(r_0 - r_{0c}, u_0, L, \rho, K_{i,j}, \tilde{a})$. As we are interested only in the singular part, we subtract the nonsingular bulk part

up to linear order in $r_0 - r_{0c}$:

$$\begin{aligned} f_{\text{ns}}^{(1)}(r_0 - r_{0c}, K_{i,j}, \tilde{a}) &= -\frac{\ln(2\pi)}{2\tilde{a}^d} + \frac{1}{2} \int_{\mathbf{k}} \ln\{\delta \hat{K}(\mathbf{k})\} \tilde{a}^2 \\ &\quad + \frac{r_0 - r_{0c}}{2} \int_{\mathbf{k}} [\delta \hat{K}(\mathbf{k})]^{-1}. \end{aligned} \quad (4.29)$$

The remaining function

$$\begin{aligned} \delta f(r_0 - r_{0c}, u_0, L, \rho, K_{i,j}, \tilde{a}) \\ = \hat{f}(r_0 - r_{0c}, u_0, L, \rho, K_{i,j}, \tilde{a}) - f_{\text{ns}}^{(1)}(r_0 - r_{0c}, K_{i,j}, \tilde{a}) \end{aligned} \quad (4.30)$$

has a finite limit for $\tilde{a} \rightarrow 0$ at fixed $r_0 - r_{0c}$ in $2 < d < 4$ dimensions,

$$\lim_{\tilde{a} \rightarrow 0} \delta f(r_0 - r_{0c}, u_0, L, \rho, K_{i,j}, \tilde{a}) = \delta f(r_0 - r_{0c}, u_0, L, \rho), \quad (4.31)$$

where we have assumed the interaction (2.19). (For the justification of taking the limit $\tilde{a} \rightarrow 0$, see the remarks after Eq. (4.36) of [7].) The function (4.31) still contains a non-singular bulk part $f_{\text{ns}}^{(2)}(r_0 - r_{0c}, u_0)$ proportional to $(r_0 - r_{0c})^2$. It is convenient to subtract this nonsingular bulk part later within the renormalized theory in the asymptotic critical region as described in Sec. IV E. Our perturbation result for the function $\delta f(r_0 - r_{0c}, u_0, L, \rho)$, as derived from (4.8)–(4.14) and (4.19)–(4.31), reads as

$$\begin{aligned} \delta f(r_0 - r_{0c}, u_0, L, \rho) &= -\frac{A_d}{r_{0L}^{\varepsilon/2}} \left[\frac{r_{0L}^2}{4d} + \frac{(r_0 - r_{0c})^2}{4\varepsilon} - 18u_0^2 M_0^4 \right] \\ &\quad + \frac{1}{L^d} \left\{ -\rho^{d-1} \ln \int_{-\infty}^\infty dz \exp\left(-\frac{1}{2} y_0^{\text{eff}}(\rho) z^2 - z^4\right) \right. \\ &\quad - \frac{1}{2} \ln \left[\frac{2\pi w_0^{\text{eff}}(\rho)}{L^{\varepsilon/2} \rho^{(d-1)/2}} \right] + \frac{1}{2} J_0(r_{0L} L^2, \rho) \\ &\quad - \frac{3u_0 M_0^2 L^2}{2\pi^2} I_1(r_{0L} L^2, \rho) - \frac{9u_0^2 M_0^4 L^4}{4\pi^4} I_2(r_{0L} L^2, \rho) \left. \right\} \\ &\quad + \frac{1 - \rho^{d-1}}{L^d} \left\{ \frac{1}{2} \ln \left[\frac{w_0^{\text{eff}}(\rho) r_{0L} L^2}{L^{\varepsilon/2} \rho^{(d-1)/2} 2\pi} \right] \right. \\ &\quad - \frac{6u_0 M_0^2}{r_{0L}} - \frac{36u_0^2 M_0^4}{r_{0L}^2} \left. \right\}, \end{aligned} \quad (4.32)$$

$$\begin{aligned} y_0^{\text{eff}}(\rho) &= \frac{L^{d/2} \rho^{(1-d)/2}}{u_0^{1/2}} \left\{ (r_0 - r_{0c}) \left[1 + 18u_0 \left(\frac{A_d(d-2)}{2\varepsilon r_{0L}^{\varepsilon/2}} \right. \right. \right. \\ &\quad + \frac{1 - \rho^{d-1}}{L^d r_{0L}^2} + \frac{L^\varepsilon}{16\pi^4} I_2(r_{0L} L^2, \rho) \left. \left. \right) \right] \\ &\quad + 12u_0 \left[-\frac{A_d}{\varepsilon r_{0L}^{(2-d)/2}} + \frac{1 - \rho^{d-1}}{L^d r_{0L}} \right. \\ &\quad + \frac{L^{2-d}}{4\pi^2} I_1(r_{0L} L^2, \rho) \left. \right] + 144u_0^2 M_0^2 \left[\frac{A_d(d-2)}{2\varepsilon r_{0L}^{\varepsilon/2}} \right. \\ &\quad + \frac{1 - \rho^{d-1}}{L^d r_{0L}^2} + \frac{L^\varepsilon}{16\pi^4} I_2(r_{0L} L^2, \rho) \left. \right] \left. \right\}, \end{aligned} \quad (4.33)$$

$$w_0^{\text{eff}}(\rho) = u_0^{-1/2} \left\{ 1 + 18u_0 \left[\frac{A_d(d-2)}{2\varepsilon} r_{0L}^{-\varepsilon/2} + \frac{1-\rho^{d-1}}{L^d} r_{0L}^{-2} + \frac{L^\varepsilon}{16\pi^4} I_2(r_{0L} L^2, \rho) \right] \right\}, \quad (4.34)$$

where now r_{0L} and M_0^2 are abbreviations for

$$r_{0L}(r_0 - r_{0c}, u_0, L, \rho) = r_0 - r_{0c} + 12u_0 M_0^2 \quad (4.35)$$

and

$$M_0^2(r_0 - r_{0c}, u_0, L, \rho) = (L^d \rho^{1-d} u_0)^{-1/2} \vartheta_2(\hat{y}_0), \quad (4.36)$$

with

$$\hat{y}_0 = (r_0 - r_{0c})(L^d \rho^{1-d} / u_0)^{1/2}. \quad (4.37)$$

Our Eqs. (4.32)–(4.37) are applicable to some finite range of $0 < \rho < \infty$ and contain Eqs. (4.37)–(4.42) of [7] as a special case for $\rho = 1$. They are not applicable to the film ($\rho \rightarrow 0$) and cylinder ($\rho \rightarrow \infty$) limits below bulk T_c .

D. Minimal renormalization at fixed dimension

As is well known, the bare perturbation form of δf requires additive and multiplicative renormalizations. As the ultraviolet behavior of δf does not depend on the aspect ratio ρ , the renormalizations are the same as those described in [7] in terms of the minimal renormalization at fixed dimension $2 < d < 4$ [35]. The adequacy of this method in combination with the geometric factor A_d [Eq. (3.5)] has been demonstrated in [7] for the case of cubic geometry. Since the aspect ratio ρ is not renormalized, we apply the same renormalizations to the present bare expression for δf [Eq. (4.32)]. The details are parallel to those in [7], which justifies us to turn directly to the renormalized form of δf . It is defined as

$$f_R(r, u, L, \rho, \mu) = \delta f(Z_r r, \mu^\varepsilon Z_u Z_\varphi^{-2} A_d^{-1} u, L, \rho, \mu) - \frac{1}{8} \mu^{-\varepsilon} r^2 A_d A(u, \varepsilon), \quad (4.38)$$

where r and u are the renormalized counterparts of $r_0 - r_{0c}$ and u_0 . For the Z factors $Z_i(u, \varepsilon)$ and the additive renormalization constant $A(u, \varepsilon)$, we refer to [7]. The inverse reference length μ is chosen as $\mu^{-1} = \xi_{0+}$, where ξ_{0+} is the asymptotic amplitude of the second-moment bulk correlation length above T_c .

The critical behavior is expressed in terms of a flow parameter $l(t, L, \rho)$, which is determined implicitly by

$$r_L(l) = \mu^2 l^2. \quad (4.39)$$

The reason for this choice of the flow parameter is given after (4.45) below. The dependence of l on t , L , and ρ enters through the function $r_L(l)$, which is the renormalized counterpart of r_{0L} . It is given by

$$\begin{aligned} r_L(l) &\equiv r_{0L}[r(l), l^\varepsilon \mu^\varepsilon A_d^{-1} u(l), L, \rho] \\ &= r(l) + 12[(\mu l)^\varepsilon A_d^{-1} u(l) L^{-d} \rho^{(d-1)}]^{1/2} \vartheta_2[y(l)] \end{aligned} \quad (4.40)$$

with

$$y(l) = r(l) \mu^{-2} l^{-2} (L \mu l)^{d/2} \rho^{(1-d)/2} A_d^{1/2} u(l)^{-1/2}, \quad (4.41)$$

where $\vartheta_2(y)$ is defined by (4.22). The effective renormalized quantities $r(l)$ and $u(l)$ are defined as usual [35]. Both $r_L(l)$ and

$y(l)$ depend on t , L , and ρ . The t dependence originates from $r(l)$, which depends on t through its initial value $r(1) = r = at$ with $a = Z_r(u, \varepsilon)^{-1} a_0$.

The effective renormalized counterparts of $y_0^{\text{eff}}(\rho)$ and of $w_0^{\text{eff}}(\rho)$ are given by

$$\begin{aligned} y^{\text{eff}}(l, \rho) &= (l \mu L)^{d/2} \rho^{(1-d)/2} A_d^{1/2} u(l)^{-1/2} \\ &\times \left\{ \frac{r(l)}{\mu^2 l^2} \left[1 + 18u(l) R_2 \left(\frac{r_L(l)}{\mu^2 l^2}, l \mu L, \rho \right) \right] \right. \\ &+ 12u(l) R_1 \left(\frac{r_L(l)}{\mu^2 l^2}, l \mu L, \rho \right) \\ &+ 144(l \mu L)^{-d/2} \rho^{(d-1)/2} A_d^{-1/2} u(l)^{3/2} \vartheta_2[y(l)] \\ &\left. \times R_2 \left(\frac{r_L(l)}{\mu^2 l^2}, l \mu L, \rho \right) \right\} \end{aligned} \quad (4.42)$$

and

$$w^{\text{eff}}(l, \rho) = u(l)^{-1/2} \left[1 + 18u(l) R_2 \left(\frac{r_L(l)}{\mu^2 l^2}, l \mu L, \rho \right) \right], \quad (4.43)$$

where

$$\begin{aligned} R_1(q, p, \rho) &= \varepsilon^{-1} q [1 - q^{-\varepsilon/2}] + A_d^{-1} (1 - \rho^{d-1}) q^{-1} p^{-d} \\ &+ p^{\varepsilon-2} (4\pi^2 A_d)^{-1} I_1(q p^2, \rho), \end{aligned} \quad (4.44)$$

$$\begin{aligned} R_2(q, p, \rho) &= -\varepsilon^{-1} [1 - q^{-\varepsilon/2}] - \frac{1}{2} q^{-\varepsilon/2} + A_d^{-1} (1 - \rho^{d-1}) \\ &\times q^{-2} p^{-d} + p^\varepsilon (16\pi^4 A_d)^{-1} I_2(q p^2, \rho), \end{aligned} \quad (4.45)$$

with I_m defined by (4.27). The dependence of the functions R_i on the ratio $r_L(l)/(\mu^2 l^2)$ is the reason for the choice (4.39) of the flow parameter. It ensures the standard choice in the bulk limit both above and below T_c [35]:

$$\lim_{L \rightarrow \infty} \lim_{l \rightarrow \infty} \mu^2 l^2 = \begin{cases} \mu^2 l_+^2 = r(l_+) & \text{for } T > T_c, \\ \mu^2 l_-^2 = -2r(l_-) & \text{for } T < T_c, \end{cases} \quad (4.46)$$

and implies $\mu l \propto L^{-1} \rho^{(d-1)/d}$ for large finite V at $T = T_c$.

After integration of the renormalization-group equation [see Eqs. (5.6) and (5.7) of [7]], the renormalized free energy density attains the structure

$$\begin{aligned} f_R(r, u, L, \rho, \mu) &= f_R[r(l), u(l), l \mu, L, \rho] + \frac{A_d r(l)^2}{2(l \mu)^\varepsilon} \int_1^l B[u(l')] \\ &\times \left\{ \exp \int_l^{l'} (2\zeta_r[u(l'')]) - \varepsilon \right\} \frac{dl''}{l''}, \end{aligned} \quad (4.47)$$

where $B(u)$ and $\zeta_r(u)$ are well-known field-theoretic functions of bulk theory [7, 35]. From (4.32) and (4.38), we derive the

first term on the right-hand side of (4.47) as

$$\begin{aligned}
 f_R[r(l), u(l), l\mu, L, \rho] &= -A_d(l\mu)^d/(4d) + 18u(l)L^{-d}\rho^{d-1}\{\vartheta_2[y(l)]\}^2 \\
 &+ \frac{1}{L^d} \left\{ -\rho^{d-1} \ln \int_{-\infty}^{\infty} dz \exp \left[-\frac{1}{2} y^{\text{eff}}(l, \rho) z^2 - z^4 \right] \right. \\
 &- \frac{1}{2} \ln \left[\frac{2\pi A_d^{1/2} w^{\text{eff}}(l, \rho)}{(l\mu L)^{\varepsilon/2} \rho^{(d-1)/2}} \right] + \frac{1}{2} J_0(l^2 \mu^2 L^2, \rho) \\
 &- \frac{3(l\mu L)^{\varepsilon/2} \rho^{(d-1)/2} u(l)^{1/2}}{2\pi^2 A_d^{1/2}} \vartheta_2[y(l)] I_1(l^2 \mu^2 L^2, \rho) \\
 &- \frac{9(l\mu L)^{\varepsilon} \rho^{d-1} u(l)}{4\pi^4 A_d} \{\vartheta_2[y(l)]\}^2 I_2(l^2 \mu^2 L^2, \rho) \left. \right\} \\
 &+ \frac{1 - \rho^{d-1}}{L^d} \left\{ \frac{1}{2} \ln \left[\frac{A_d^{1/2} w^{\text{eff}}(l, \rho) l^2 \mu^2 L^2}{(l\mu L)^{\varepsilon/2} \rho^{(d-1)/2} 2\pi} \right] \right. \\
 &- 6u(l)^{1/2} (l\mu L)^{-d/2} \rho^{(d-1)/2} A_d^{-1/2} \vartheta_2[y(l)] \\
 &- 36u(l)(l\mu L)^{-d} \rho^{d-1} A_d^{-1} \{\vartheta_2[y(l)]\}^2 \left. \right\}. \quad (4.48)
 \end{aligned}$$

E. Finite-size scaling function of the free energy density

It is straightforward to show that the asymptotic form (2.23) of the singular part f_s of the free energy density is obtained from f_R [Eq. (4.47)] in the limit of small $l \ll 1$ or $l \rightarrow 0$ as

$$f_R \rightarrow f_s(t, L, L_{\parallel}) = L^{-d} F(\tilde{x}, \rho) \quad (4.49)$$

with the scaling variable \tilde{x} [Eq. (2.24)]. In this limit, we have $u(l) \rightarrow u(0) \equiv u^*$, $r(l)/(\mu^2 l^2) \rightarrow Q^* t l^{-1/\nu}$,

$$y(l) \rightarrow \tilde{y} = \tilde{x} Q^* (\mu l L)^{-\alpha/(2\nu)} \rho^{(1-d)/2} A_d^{1/2} u^{*-1/2}, \quad (4.50)$$

and $\mu l L \rightarrow \tilde{l} = \tilde{l}(\tilde{x}, \rho)$, where the function $\tilde{l}(\tilde{x}, \rho)$ is determined implicitly by

$$\tilde{y} + 12\vartheta_2(\tilde{y}) = \rho^{(1-d)/2} \tilde{l}^{d/2} A_d^{1/2} u^{*-1/2}, \quad (4.51)$$

$$\tilde{y} = \tilde{x} Q^* \tilde{l}^{-\alpha/(2\nu)} \rho^{(1-d)/2} A_d^{1/2} u^{*-1/2}. \quad (4.52)$$

These two equations also determine $\tilde{y} = \tilde{y}(\tilde{x}, \rho)$. In Eqs. (4.50)–(4.52), we have used the hyperscaling relation $2 - \alpha = d\nu$. The factor $Q^* = Q(1, u^*, d)$ is the fixed point value of the amplitude function $Q(1, u, d)$ of the bulk correlation length above T_c [7, 31, 35, 43]. Furthermore, we have, in the small- l limit,

$$w^{\text{eff}}(l, \rho) \rightarrow W(\tilde{x}, \rho) = u^{*-1/2} [1 + 18u^* R_2(1, \tilde{l}, \rho)], \quad (4.53)$$

$$\begin{aligned}
 y^{\text{eff}}(l, \rho) \rightarrow Y(\tilde{x}, \rho) &= \tilde{l}^{d/2} \rho^{(1-d)/2} A_d^{1/2} u^{*-1/2} \left\{ Q^* \tilde{x} \tilde{l}^{-1/\nu} \right. \\
 &\times [1 + 18u^* R_2(1, \tilde{l}, \rho)] + 12u^* R_1(1, \tilde{l}, \rho) \\
 &+ 144[u^* \tilde{l}^{-d} \rho^{(d-1)} A_d^{-1}]^{1/2} \\
 &\left. \times \vartheta_2(\tilde{y}) R_2(1, \tilde{l}, \rho) \right\}. \quad (4.54)
 \end{aligned}$$

For $l \ll 1$, the last integral term in (4.47) contains both a contribution $\propto t^2 l^{-\alpha/\nu}$ to the singular finite-size part $f_s(t, L, L_{\parallel})$ and a contribution $\propto t^2$ to the nonsingular bulk part $f_{\text{ns},b}^{(2)}$ of

δf mentioned after (4.31) [see also the comment on Eq. (6.8) of [7]]. This nonsingular part will be neglected in the following.

Equations (4.47), (4.48), and (4.49)–(4.54) lead to the finite-size scaling function

$$\begin{aligned}
 F(\tilde{x}, \rho) &= -A_d \left[\frac{\tilde{l}^d}{4d} + \frac{\nu Q^{*2} \tilde{x}^2 \tilde{l}^{-\alpha/\nu}}{2\alpha} B(u^*) \right] \\
 &+ 18u^* \rho^{d-1} [\vartheta_2(\tilde{y})]^2 - \frac{1}{2} \ln \left(\frac{2\pi A_d^{1/2} W(\tilde{x}, \rho)}{\tilde{l}^{\varepsilon/2} \rho^{(d-1)/2}} \right) \\
 &- \rho^{d-1} \ln \int_{-\infty}^{\infty} dz \exp \left[-\frac{1}{2} Y(\tilde{x}, \rho) z^2 - z^4 \right] \\
 &+ \frac{1}{2} J_0(\tilde{l}^2, \rho) - \frac{3\tilde{l}^{\varepsilon/2} u^{*1/2} \rho^{(d-1)/2}}{2\pi^2 A_d^{1/2}} \vartheta_2(\tilde{y}) I_1(\tilde{l}^2, \rho) \\
 &- \frac{9\tilde{l}^{\varepsilon} u^* \rho^{d-1}}{4\pi^4 A_d} [\vartheta_2(\tilde{y})]^2 I_2(\tilde{l}^2, \rho) + (1 - \rho^{d-1}) \\
 &\times \left\{ \frac{1}{2} \ln \left[\frac{A_d^{1/2} W(\tilde{x}, \rho) \tilde{l}^{d/2}}{2\pi \rho^{(d-1)/2}} \right] - 6u^{*1/2} \tilde{l}^{-d/2} \rho^{(d-1)/2} \right. \\
 &\left. \times A_d^{-1/2} \vartheta_2(\tilde{y}) - 36u^* \tilde{l}^{-d} \rho^{d-1} A_d^{-1} [\vartheta_2(\tilde{y})]^2 \right\} \quad (4.55)
 \end{aligned}$$

with A_d , J_0 , I_m , and ϑ_2 defined in (3.5), (4.26), (4.27), and (4.22), respectively. Equation (4.55) is the central analytic result of this paper for the case $n = 1$. It is valid for $2 < d < 4$ in the central finite-size regime (between the dashed lines of Fig. 2), i.e., in the range $L \gg \tilde{a}$, $L_{\parallel} \gg \tilde{a}$, and $0 \leq |\tilde{x}| \lesssim O(1)$ above, at, and below T_c for finite ρ . For the special case $\rho = 1$, Eq. (4.55) is identical with Eq. (6.10) of [7]. For $d = 3$, Eq. (4.55) reduces to Eq. (9) presented in [24]. It incorporates the correct bulk critical exponents α and ν and the complete bulk function $B(u^*)$ (not only in one-loop order). The Borel resummed values of the fixed point value u^* [44], of $B(u^*)$ [44], and of Q^* [31, 35, 43] in three dimensions are given after Eq. (5.5) below. There is only one adjustable parameter that is contained in the nonuniversal bulk amplitude ξ_{0+} of the scaling variable \tilde{x} . For finite L and L_{\parallel} , $f_s(t, L, L_{\parallel})$ is an analytic function of t near $t = 0$, i.e., $F(\tilde{x}, \rho)$ is an analytic function of \tilde{x} near $\tilde{x} = 0$ at finite ρ , in agreement with general analyticity requirements.

The bulk part $F_b^{\pm}(\tilde{x})$ of $F(\tilde{x}, \rho)$ is obtained from (4.55) in the large- $|\tilde{x}|$ limit. It is represented by (2.25), with the universal bulk amplitude ratios

$$Q_1 = -A_d Q^{*d\nu} \left[\frac{1}{4d} + \frac{\nu}{2\alpha} B(u^*) \right], \quad (4.56)$$

$$\frac{A^-}{A^+} = 2^{d\nu} \frac{1/(64u^*) + 1/(4d) + 81u^*/64 + \nu B(u^*)/(8\alpha)}{1/(4d) + \nu B(u^*)/(2\alpha)} \quad (4.57)$$

given by Eqs. (6.19) and (6.20) of [7]. We then obtain from (4.55) the scaling function $F^{\text{ex}}(\tilde{x}, \rho)$ [Eq. (2.27)] of the excess free energy density, which determines the scaling function $X(\tilde{x}, \rho)$ of the Casimir force according to (2.29). By

definition, the functions $F^{ex}(\tilde{x}, \rho)$ and $X(\tilde{x}, \rho)$ have a weak singularity at $\tilde{x} = 0$ arising from the subtraction of the bulk term $F_b^\pm(\tilde{x})$.

V. QUANTITATIVE RESULTS IN THREE DIMENSIONS IN THE CENTRAL FINITE-SIZE REGIME

A. Amplitudes at T_c and monotonicity hypothesis

Of particular interest is the finite-size amplitude at T_c :

$$\begin{aligned}
 F(0, \rho) &= \left(18 - \frac{36}{d}\right) u^* \rho^{d-1} [\vartheta_2(0)]^2 \\
 &\quad - \frac{1}{2} \ln \left(\frac{2\pi A_d^{1/2} W_c(\rho)}{\tilde{l}_c^{e/2} \rho^{(d-1)/2}} \right) - \rho^{d-1} \ln \int_{-\infty}^{\infty} dz \\
 &\quad \times \exp \left[-\frac{1}{2} Y_c(\rho) z^2 - z^4 \right] + \frac{1}{2} J_0(\tilde{l}_c^2, \rho) - \frac{\tilde{l}_c^2}{8\pi^2} I_1(\tilde{l}_c^2, \rho) \\
 &\quad - \frac{\tilde{l}_c^4}{64\pi^4} I_2(\tilde{l}_c^2, \rho) + (1 - \rho^{d-1}) \\
 &\quad \times \left\{ \frac{1}{2} \ln \left[\frac{A_d^{1/2} W_c(\rho) \tilde{l}_c^{d/2}}{2\pi \rho^{(d-1)/2}} \right] - \frac{3}{4} \right\}, \quad (5.1)
 \end{aligned}$$

where $\tilde{l}_c^{d/2} = 12u^{*1/2} \rho^{(d-1)/2} A_d^{-1/2} \vartheta_2(0)$ and

$$W(0, \rho) \equiv W_c(\rho) = u^{*-1/2} [1 + 18 u^* R_2(1, \tilde{l}_c, \rho)], \quad (5.2)$$

$$Y(0, \rho) \equiv Y_c(\rho) = 144u^* \vartheta_2(0) \{R_1(1, \tilde{l}_c, \rho) + R_2(1, \tilde{l}_c, \rho)\} \quad (5.3)$$

with $\vartheta_2(0) = \Gamma(3/4)/\Gamma(1/4)$ and

$$R_1(1, \tilde{l}_c, \rho) = \frac{\tilde{l}_c^{-d}}{4\pi^2 A_d} I_1(\tilde{l}_c^2, \rho) + A_d^{-1} (1 - \rho^{d-1}) \tilde{l}_c^{-d}, \quad (5.4)$$

$$R_2(1, \tilde{l}_c, \rho) = -\frac{1}{2} + \frac{\tilde{l}_c^e}{16\pi^4 A_d} I_2(\tilde{l}_c^2, \rho) + A_d^{-1} (1 - \rho^{d-1}) \tilde{l}_c^{-d}. \quad (5.5)$$

For the application to three dimensions, we shall employ the following numerical values [7,31,45]: $A_3 = (4\pi)^{-1}$, $v = 0.6335$, $u^* = 0.0412$, $Q^* = 0.945$, $B(u^*) = 0.50$, and $\alpha = 2 - 3v = 0.0995$. At T_c in three dimensions, the ρ dependence of the flow parameter is given by

$$\tilde{l}_c = [12(4\pi u^*)^{1/2} \Gamma(3/4)/\Gamma(1/4)]^{2/3} \rho^{2/3} = 2.042 \rho^{2/3}. \quad (5.6)$$

The ρ dependence of the integrals $J_0(\tilde{l}_c^2, \rho)$ [Eq. (4.26)] and $I_m(\tilde{l}_c^2, \rho)$ [Eq. (4.27)] needs to be computed numerically. The resulting amplitudes $F(0, \rho)$, $X(0, \rho)$, $\Phi(0, \rho)$, and $\Xi(0, \rho)$ as determined by (5.1), (5.10), (2.39), and (5.11) are shown by the thick lines in Figs. 5 and 6, respectively, in a finite range of ρ and $1/\rho$. At $\rho = 1$, perfect agreement with the MC data by Mon [41] [full circle in Figs. 5(a) and 6(a)] is found.

Figures 5 and 6 demonstrate the weakness of the n dependence at T_c . On the basis of the monotonicity of the curves for the case $n = \infty$ (thin curves in Figs. 5 and 6), we

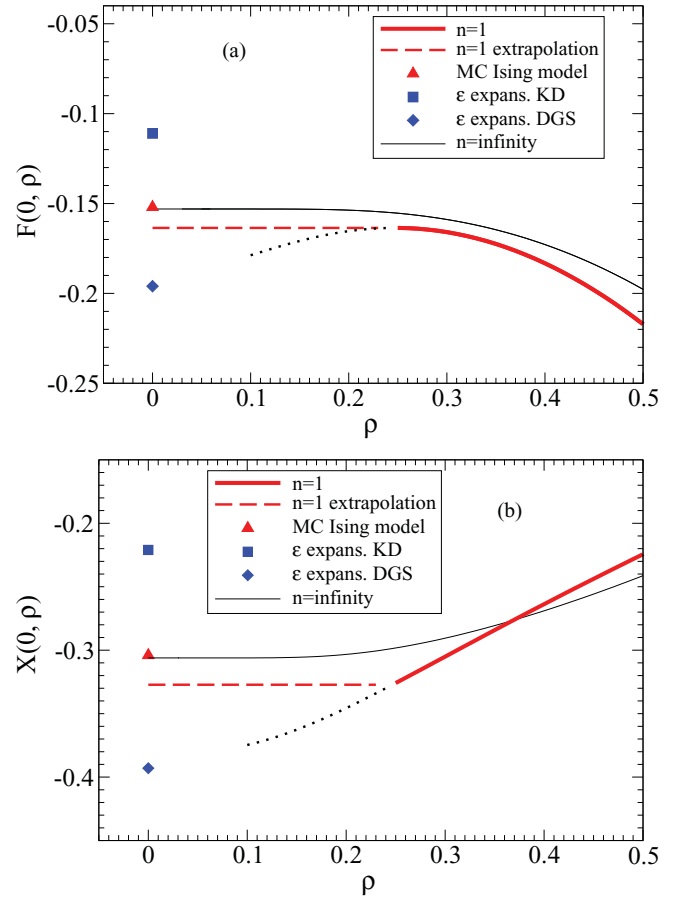


FIG. 7. (Color online) Critical amplitudes (a) $F(0, \rho)$ [Eq. (2.27)] and (b) $X(0, \rho)$ [Eq. (5.10)] at T_c in three dimensions as a function of the aspect ratio ρ for $n = 1$ [thick lines, from (5.1)] and in the large- n limit [thin lines, from (3.6)]. The maximum -0.1636 of the $n = 1$ line in (a) is at $\rho_{\max} = 0.2470$. The dashed lines are the extrapolations of the $n = 1$ lines from $\rho = \rho_{\max}$ to $\rho = 0$ corresponding to film geometry. The dotted lines represent (5.1) in the regime $\rho < \rho_{\max}$, where our perturbation theory is not applicable. The MC estimate for the $d = 3$ Ising model from [16] (triangles), ϵ expansion results for $n = 1$ from [19] (squares), and from [20] (diamonds). See also Fig. 5.

expect monotonicity also for the $n = 1$ curves. As shown in the magnified plots of Figs. 7(a) and 8(a), $F(0, \rho)$ and $\Phi(0, \rho)$ indeed have the expected monotonic behavior, but only in the restricted range $\rho \geq \rho_{\max} = 0.2470$ and $1/\rho \geq (1/\rho)_{\max} = 0.3223$, respectively. As expected on general grounds, the lowest-mode separation approach should fail for sufficiently small $\rho < \rho_{\max}$ or $1/\rho < (1/\rho)_{\max}$, respectively, near the film and the cylinder limit (dotted lines in Figs. 7 and 8), where the higher modes are no longer well separated from the single lowest mode. Thus, our hypothesis of monotonicity provides the following quantitative estimate for the range of the aspect ratio ρ within which our lowest-mode separation approach for the free energy is expected to be reliable:

$$1/4 \lesssim \rho \lesssim 3. \quad (5.7)$$

Furthermore, we expect a negligible dependence on ρ and $1/\rho$ in the range $\rho < \rho_{\max}$ or $1/\rho < (1/\rho)_{\max}$, respectively, corresponding to the extrapolations (dashed lines) in Figs. 7(a)

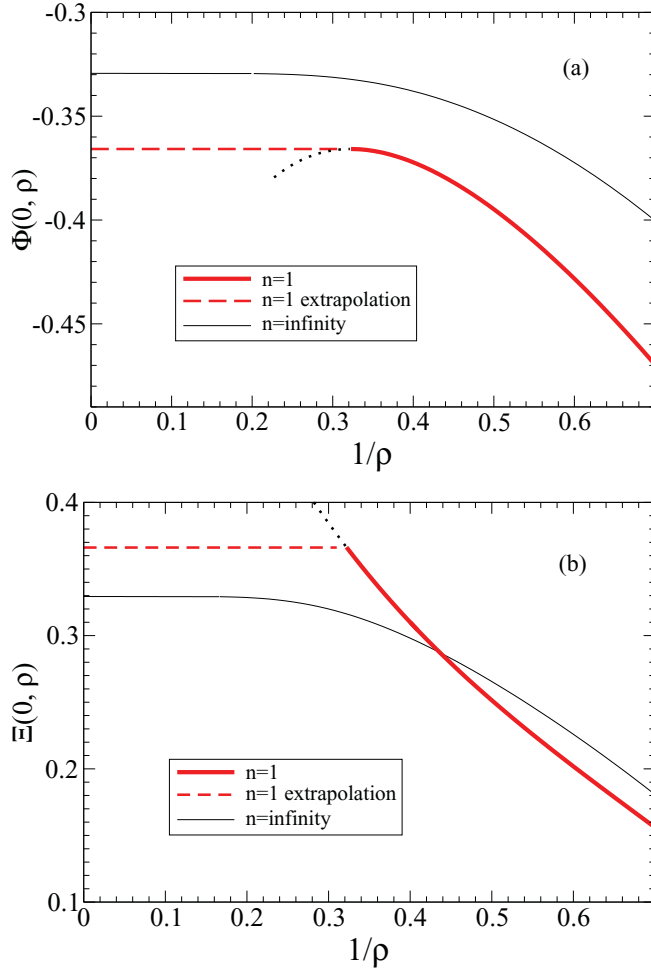


FIG. 8. (Color online) Critical amplitudes (a) $\Phi(0, \rho)$ [Eq. (2.39)] and (b) $\Xi(0, \rho)$ [Eq. (5.11)] at T_c in three dimensions as a function of the inverse aspect ratio $1/\rho$ for $n = 1$ [thick lines, from (5.1)] and in the large- n limit [thin lines, from (3.6)]. The maximum -0.3658 of the $n = 1$ line in (a) is at $(1/\rho)_{\max} = 0.3223$. The dashed lines are the extrapolations of the $n = 1$ lines from $(1/\rho)_{\max}$ to $1/\rho = 0$ corresponding to cylinder geometry. The dotted lines represent (5.1) in the regime of small $1/\rho < (1/\rho)_{\max}$, where our perturbation theory is not applicable. See also Fig. 6.

and 8(a). This leads to our prediction of the $n = 1$ amplitudes of the scaling functions of the excess free energy density at bulk T_c for the film and for the cylinder in three dimensions:

$$F_{\text{film}}(0) \approx F(0, \rho = 1/4) = -0.164, \quad (5.8)$$

$$\Phi_{\text{cyl}}(0) \approx \Phi(0, \rho = 3) = -0.366. \quad (5.9)$$

The corresponding results for the Casimir amplitudes $X(0, \rho)$ and $\Xi(0, \rho)$ are shown in Figs. 7(b) and 8(b); they follow from those of $F(0, \rho)$ and $\Phi(0, \rho)$ by means of the exact relations [compare (2.29) and (2.41)]

$$X(0, \rho) = (d-1)F(0, \rho) - \rho \frac{\partial F(0, \rho)}{\partial \rho}, \quad (5.10)$$

$$\Xi(0, \rho) = -\Phi(0, \rho) + (1/\rho) \frac{\partial \Phi(0, \rho)}{\partial (1/\rho)}. \quad (5.11)$$

From (5.8) and (5.9), we obtain our prediction of the $n = 1$ amplitudes of the Casimir force scaling functions at bulk T_c for the film and for the cylinder in three dimensions [dashed lines in Figs. 7(b) and 8(b)]:

$$X_{\text{film}}(0) \equiv X(0, 0) = 2F_{\text{film}}(0) = -0.328, \quad (5.12)$$

$$\Xi_{\text{cyl}}(0) \equiv \Xi(0, \infty) = -\Phi_{\text{cyl}}(0) = 0.366. \quad (5.13)$$

Our results for $F_{\text{film}}(0)$ and $X_{\text{film}}(0)$ are in good agreement with the MC estimates [16] $\Delta_P = -0.152$ and $2\Delta_P = -0.304$ [triangles in Fig. 7] for the three-dimensional Ising model in film geometry at bulk T_c . The previous ε expansion results up to $O(\varepsilon)$ [19] [squares in Fig. 7], and up to $O(\varepsilon^{3/2})$ [20] [diamonds in Fig. 7], are in less good agreement with the MC estimates.

It would be interesting to test our predictions for $\Phi_{\text{cyl}}(0)$ [Eq. (5.9)] and $\Xi_{\text{cyl}}(0)$ [Eq. (5.13)] by MC simulations for the three-dimensional Ising model in cylinder geometry.

B. Finite-size scaling functions

Now we turn to a discussion of the temperature dependence. In Figs. 9 and 10, we show the scaling functions $F^{\text{ex}}(\tilde{x}, \rho)$, $X(\tilde{x}, \rho)$, $\Phi^{\text{ex}}(\tilde{x}_{\parallel}, \rho)$, and $\Xi(\tilde{x}_{\parallel}, \rho)$ for $n = 1$ in three dimensions for slab, cube, and rod geometries, respectively, with finite aspect ratios in the range $1/4 \leq \rho \leq 5/2$, as derived from (4.55), (2.27), (2.29), (2.40), and (2.41). It is expected that these curves are applicable to the central finite-size regime $|\tilde{x}| \lesssim O(1)$ and $|\tilde{x}_{\parallel}| \lesssim O(1)$ but not to $|\tilde{x}| \gg 1$ and $|\tilde{x}_{\parallel}| \gg 1$. (For a more precise estimate, see below.) Figures 9 and 10 should be compared with the corresponding Figs. 3 and 4 for the case $n = \infty$.

We see that there are significant differences between the cases $n = 1$ and ∞ . Figures 9(a) and 10(a) exhibit a nonmonotonicity of $F^{\text{ex}}(\tilde{x}, \rho)$ and $\Phi^{\text{ex}}(\tilde{x}_{\parallel}, \rho)$ for $n = 1$ with minima slightly below T_c for all ρ . Such minima should also persist in the $n = 1$ film ($\rho = 0$) system and in the $n = 1$ cylinder ($1/\rho = 0$) system, the scaling functions of which should be close to our curves for $\rho = 1/4$ and $1/\rho = 2/5$, respectively. There is no good agreement at T_c between our $\rho = 1/4$ curve in Fig. 9(a) and the ε expansion results (thin lines) of [19,21] for $\rho = 0$. The latter exhibit an unphysical singularity at $\tilde{x} = 0$ (i.e., at bulk T_c) that arises from the ε expansion results [19,21] for the term $F(\tilde{x}, \rho)$ in (2.27), which should be an analytic function of \tilde{x} near $\tilde{x} = 0$ since the film transition occurs at a distinct temperature $T_{c,\text{film}}$ below bulk T_c . Our curves contain a different type of singularity at $\tilde{x} = 0$ that arises from subtracting the singular bulk part $F_b^{\pm}(\tilde{x})$ in (2.27); this singularity is very weak and not visible in Figs. 9 and 10.

In Fig. 9(b), our results show an unexpected structure of the Casimir force scaling function X near bulk T_c where local *maxima* occur with increasing $\rho > 1/4$. The small shoulder for $\rho = 1/4$ was already noticed previously [24]. This structure with local maxima does not exist for $n = \infty$. Such maxima also persist in the regime of $\rho > 1$ as shown in Fig. 10(b). As a special feature of the case $\rho = 1$, X and Ξ vanish at bulk T_c in three dimensions, as shown by double-dotted-dashed curves in Figs. 9(b) and 10(b) (see also Figs. 5 and 6). In addition, the Casimir force for $n = 1$ in a cube changes sign at $\tilde{x} = -0.884$

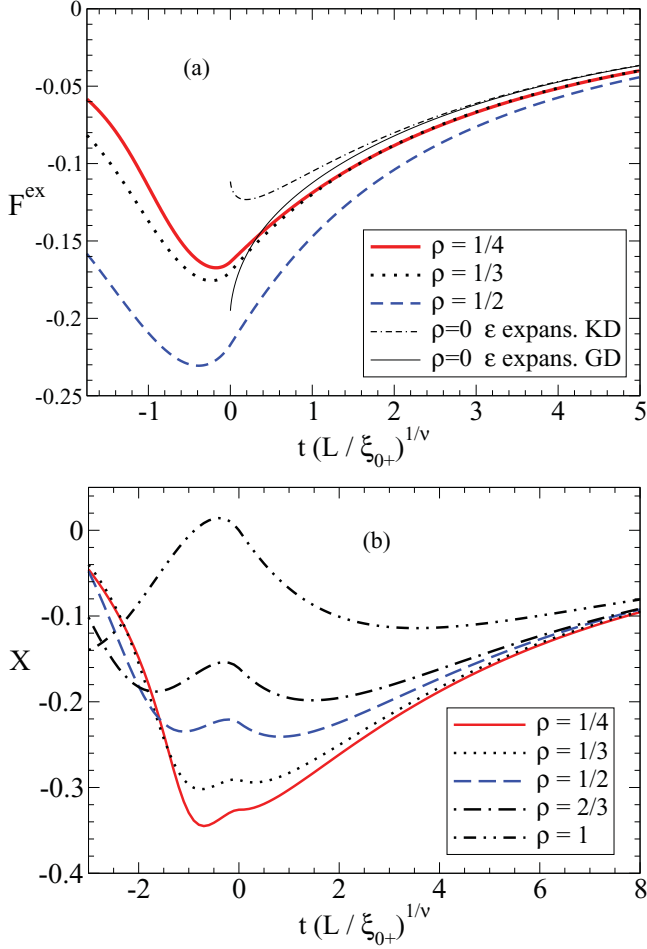


FIG. 9. (Color online) Scaling function (a) $F^{ex}(\tilde{x}, \rho)$ [Eqs. (2.27) and (4.55)] and (b) $X(\tilde{x}, \rho)$ [Eqs. (2.29), (2.27), and (4.55)] as a function of $\tilde{x} = t(L/\xi_{0+})^{1/\nu}$ for $n = 1$ in three dimensions for slab geometry with finite aspect ratio $\rho = 1/4$ (solid lines), $\rho = 1/3$ (dotted lines), $\rho = 1/2$ (dashed lines), $\rho = 2/3$ (dotted-dashed line), $\rho = 1$ (double-dotted-dashed line). Thin lines in (a): ε expansion results for $\rho = 0$ from [19,21].

and is negative for $\tilde{x} < -0.884$, contrary to the case $n = \infty$ below T_c [Figs. 3(b) and 4(b) for $\rho = 1$]. Thus, our theory predicts that, in a cube, there is only a small positive region between $\tilde{x} = -0.884$ and $\tilde{x} = 0$.

On purely theoretical grounds, it is difficult to provide a precise quantitative estimate for the range of validity of our perturbation approach with regard to the dependence on the scaling variable \tilde{x} . Valuable information, however, has been made available to us by Hasenbusch [36], who performed MC simulations for the free energy density of the three-dimensional Ising model in a cubic geometry. These data are shown in Fig. 11, together with our theoretical curve derived from (2.27) and (4.55). We see that there is good agreement in the range $-0.05 \lesssim \tilde{x} \lesssim 3$, but significant deviations exist well below T_c ; small but systematic deviations exist also well above T_c . In particular, our perturbation result for F^{ex} has an algebraic approach to a *finite* limit $F^{ex}(\infty, \rho)$ for $\tilde{x} \rightarrow \infty$, whereas there should be an exponential decay toward zero (see Sec. VI). From this comparison, it is obvious that the

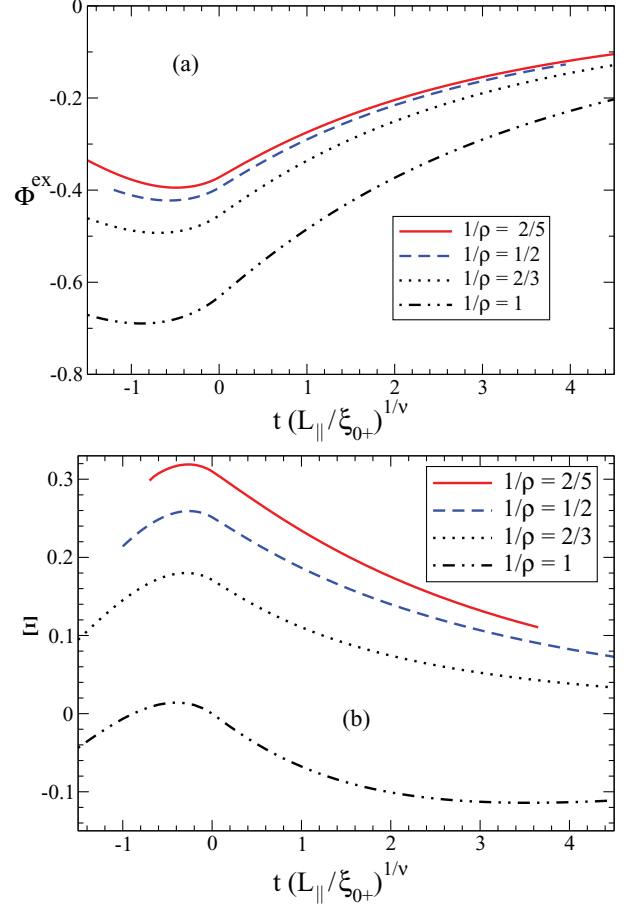


FIG. 10. (Color online) (a) Scaling function (a) $\Phi^{ex}(\tilde{x}_{||}, \rho)$ [Eqs. (2.40), (2.27), and (4.55)] and (b) $\Xi(\tilde{x}_{||}, \rho)$ [Eq. (2.41)] as a function of $\tilde{x}_{||} = t(L_{||}/\xi_{0+})^{1/\nu}$ for $n = 1$ in three dimensions for rod geometry with finite aspect ratio $1/\rho = 1$ (double-dotted-dashed lines), $1/\rho = 2/3$ (dotted lines), $1/\rho = 1/2$ (dashed lines), and $1/\rho = 2/5$ (solid lines).

lowest-mode separation approach needs to be complemented by a perturbation approach that is valid outside the central finite-size regime. Such an approach will be presented in the subsequent section.

Additional valuable information comes from a comparison of our Casimir force scaling function with earlier MC data for periodic BC in the small- ρ regime [16]. We recall that the lower limit of applicability of our calculation is $\rho = 1/4$ and that the Casimir forces should depend only weakly on ρ for $\rho < 1/4$, thus, it is reasonable to compare our result for $\rho = 1/4$ with MC data for $\rho = 1/6$ [16]. This comparison is shown in Fig. 12. Also shown are the previous ε expansion results for $\rho = 0$ from [19,21], which exhibit the same kind of singularity at $\tilde{x} = 0$ as in Fig. 9(a). We see good agreement of the MC data with our fixed d perturbation theory in the whole range $-2 \lesssim \tilde{x} \lesssim 20$. There are systematic deviations only for $\tilde{x} < -2$, which are less pronounced than those for F^{ex} in the same region. In the subsequent section, we shall explain this different degree of agreement between our theory and the MC data shown in Figs. 11 and 12.

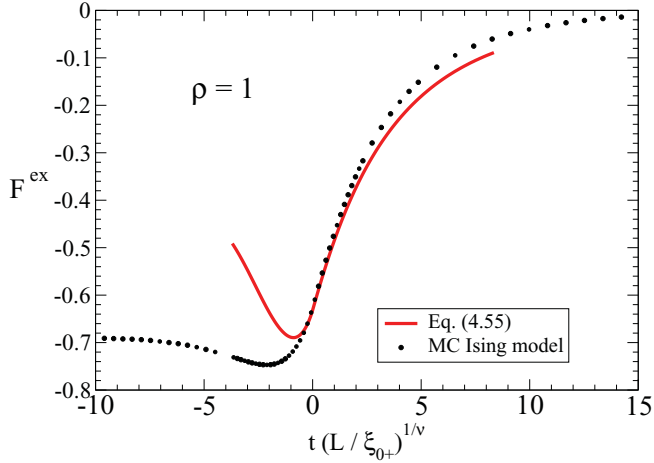


FIG. 11. (Color online) Scaling function $F^{\text{ex}}(\tilde{x}, 1)$ [Eqs. (2.27) and (4.55)] for $n = 1$ as a function of $\tilde{x} = t(L/\xi_{0+})^{1/\nu}$ in three dimensions for cubic geometry (solid line) and MC data for the $d = 3$ Ising model by Hasenbusch [36]. See also Fig. 13(c).

VI. PERTURBATION THEORY OUTSIDE THE CENTRAL FINITE-SIZE REGIME

Outside the central finite-size regime, there is no need for separating the lowest mode, thus, ordinary perturbation theory with respect to u_0 should be appropriate. By “outside the central finite-size regime” we mean the regions below the dashed lines in Fig. 2. Within these regions, it is necessary to further distinguish between scaling and nonscaling regions (the nonscaling regions correspond to the shaded regions in Fig. 2; see also Fig. 1 of [7]). The central parts of both the scaling and the nonscaling regions still belong to the asymptotic critical region $|t| \ll 1$ and $L \gg \tilde{a}$, $L_{\parallel} \gg \tilde{a}$.

Here, we perform the corresponding analysis at the one-loop level. In Secs. VIA–VIC, we shall consider the scaling region outside the central finite-size regime. The total scaling

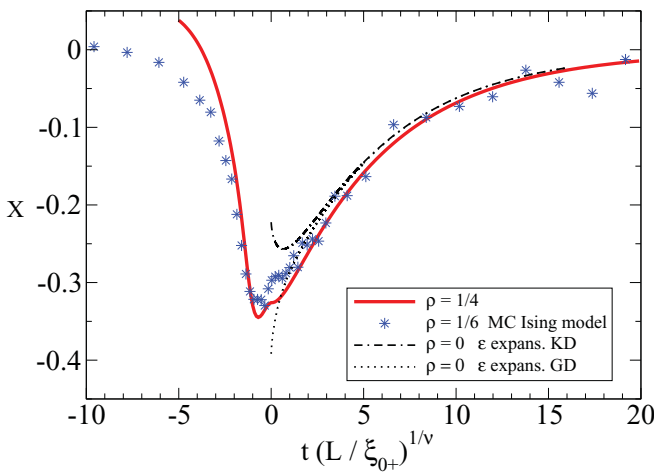


FIG. 12. (Color online) Scaling function $X(\tilde{x}, \rho)$ [Eqs. (2.29), (2.27), and (4.55)] for $n = 1$ as a function of $\tilde{x} = t(L/\xi_{0+})^{1/\nu}$ in three dimensions for slab geometry with $\rho = 1/4$ (solid line) and MC data for the $d = 3$ Ising model with $\rho = 1/6$ by Vasilyev *et al.* [16]. Thin lines: ε expansion results for $\rho = 0$ from [19,21]. See also Fig. 14(a).

region can be roughly characterized by $L/\tilde{a} \gg 1$, $L_{\parallel}/\tilde{a} \gg 1$, $\xi_{\pm}/\tilde{a} \gg 1$, and $L/\xi_{\pm} \lesssim 24(\xi_{\pm}/\tilde{a})^2$, $L_{\parallel}/\xi_{\pm} \lesssim 24(\xi_{\pm}/\tilde{a})^2$, where ξ_{\pm} is the second-moment bulk correlation length above and below T_c , respectively. (Note that this characterization also includes the central finite-size regime, which is part of the total scaling region.) The latter restrictions follow from the conditions (6.18) for the nonscaling regions that will be studied in Sec. VI D below. In order to distinguish the perturbation results of this section from those of Secs. IV and V, we use the notation $f_{1\text{-loop}}^+$, $f_{1\text{-loop}}^-$, etc.

A. Perturbation theory well above T_c

Ordinary perturbation theory for the excess free energy density (2.9) for $n = 1$ above T_c yields in one-loop order

$$f_{1\text{-loop}}^{\text{ex},+} = \frac{1}{2V} \sum_{\mathbf{k}} \ln\{[r_0 - r_{0c} + \delta\hat{K}(\mathbf{k})]\tilde{a}^2\} - \frac{1}{2} \int_{\mathbf{k}} \ln\{[r_0 - r_{0c} + \delta\hat{K}(\mathbf{k})]\tilde{a}^2\}. \quad (6.1)$$

Here, we have already replaced r_0 by $r_0 - r_{0c}$, which is justified since $r_{0c} \sim O(u_0)$ [see (4.28)]. Because of the $\mathbf{k} = \mathbf{0}$ term, the sum exists only for $r_0 - r_{0c} > 0$. The evaluation of the excess free energy density is outlined in the Appendix.

In the scaling region in $2 < d < 4$ dimensions, the large- \mathbf{k} dependence of $\delta\hat{K}(\mathbf{k})$ does not matter and the leading contribution is obtained by taking the continuum limit $\tilde{a} \rightarrow 0$ at fixed $r_0 - r_{0c} > 0$. For a renormalization-group (RG) treatment in the scaling region, see (10.5)–(10.13) of [7]. Neglecting nonasymptotic corrections to scaling, we obtain the scaling function

$$F_{1\text{-loop}}^{\text{ex},+}(\tilde{x}, \rho) = \frac{1}{2} \mathcal{G}_0(\tilde{x}^{2\nu}, \rho) + O(u^*), \quad (6.2)$$

where \mathcal{G}_0 is given by (3.7) and $\tilde{x}^\nu = L/\xi_+$, $\xi_+ = \xi_{0+}t^{-\nu}$ [for ξ_{0+} see (5.16) of [7]]. For large \tilde{x} , $F_{1\text{-loop}}^{\text{ex},+}$ decays exponentially to zero according to the asymptotic behavior

$$F_{\text{asympt}}^{\text{ex},+}(\tilde{x}, \rho) = -\left(\frac{\tilde{x}^\nu}{2\pi}\right)^{\frac{d-1}{2}} \exp(-\tilde{x}^\nu) - \rho^d(d-1)\left(\frac{\tilde{x}^\nu}{2\pi}\right)^{\frac{d-1}{2}} \exp(-\tilde{x}^\nu), \quad (6.3)$$

apart from corrections of $O(e^{-2\tilde{x}^\nu}, e^{-2\tilde{x}^\nu})$, with $\tilde{x}_{\parallel}^\nu = \tilde{x}^\nu/\rho$. Equation (6.3) follows from (A16) in the Appendix for $\xi_+/\tilde{a} \gg 1$. We see that the scaling variable \tilde{x}_{\parallel} appears in a natural way in the second term of (6.3). For $\rho = 1$, (6.2) and (6.3) agree with Eqs. (10.10)–(10.12) of [7].

The corresponding scaling functions $\Phi_{1\text{-loop}}^{\text{ex},+}$, $X_{1\text{-loop}}^+$, $\Xi_{1\text{-loop}}^+$ and $\Phi_{\text{asympt}}^{\text{ex},+}$, X_{asympt}^+ , Ξ_{asympt}^+ follow from (6.2), (6.3), (2.29), (2.40), and (2.41), respectively.

B. Perturbation theory well below T_c

Perturbation theory for *bulk* quantities below T_c within the φ^4 model for $n = 1$ at vanishing external field h may be formulated by first starting with the perturbation expression at finite external field $h > 0$ (or $h < 0$) and at finite volume $V = L_{\parallel}^{d-1}L$, then performing the thermodynamic limit $V \rightarrow \infty$ at finite $h > 0$ (or $h < 0$), and subsequently performing the zero-field limit $h \rightarrow 0_+$ (or $h \rightarrow 0_-$). Applying this

procedure to the free energy density $f(t, L, L_{\parallel}, h)$ implies that only the contributions of a *single* bulk phase with a positive (or negative) spontaneous bulk magnetization are taken into account in the calculation of

$$f_b(t) = \lim_{h \rightarrow 0+} \lim_{V \rightarrow \infty} f(t, L, L_{\parallel}, h) = \lim_{h \rightarrow 0-} \lim_{V \rightarrow \infty} f(t, L, L_{\parallel}, h). \quad (6.4)$$

In MC simulations of *finite* Ising models at vanishing external field, however, all configurations of both phases with positive and negative magnetization do contribute. In this case, the order-parameter distribution function has two finite peaks with equal heights in the positive and negative ranges of the magnetization [17,25,48,49]. For $T \rightarrow 0$, these two peaks are well separated. In order to account for this fact in an analytic treatment of the φ^4 model well below T_c , it is appropriate to formulate perturbation theory such that an expansion is made around the *two* separate peaks of the order-parameter distribution function that exist at $h = 0$.

In the following, we perform this approach at the one-loop level in order to calculate $f_{1\text{-loop}}^{ex,-}(t, L, L_{\parallel}, h = 0)$ well below T_c . First, we decompose the lattice variable φ_i of the Hamiltonian H [Eq. (2.1)] as $\varphi_i = M_{>,mf} + \delta\varphi_i$ with the *positive* mean-field order parameter $M_{>,mf} = [-r_0/(4u_0)]^{1/2} > 0$. Keeping only the Gaussian terms of H up to $O[(\delta\varphi_i)^2]$ corresponding to a one-loop approximation leads to the dimensionless partition function [compare (B1) of [7]]

$$Z_{>} = \exp\left[V \frac{r_0^2}{16u_0}\right] \prod_{\mathbf{k}} \left(\frac{2\pi}{[-2r_0 + \delta\widehat{K}(\mathbf{k})]\tilde{a}^2} \right)^{1/2}. \quad (6.5)$$

It can be rewritten as

$$Z_{>} = \exp(-V f_b^-) Z_{>}^{ex}, \quad (6.6)$$

where f_b^- is the bare bulk free energy density (4.18) in one-loop order below T_c and

$$Z_{>}^{ex} = \exp\{V \tilde{f}^{ex}\} \quad (6.7)$$

is the finite-size part of $Z_{>}$ with the contribution

$$\begin{aligned} \tilde{f}^{ex} = & \frac{1}{2V} \sum_{\mathbf{k}} \ln\{[-2r_0 + \delta\widehat{K}(\mathbf{k})]\tilde{a}^2\} \\ & - \frac{1}{2} \int_{\mathbf{k}} \ln\{[-2r_0 + \delta\widehat{K}(\mathbf{k})]\tilde{a}^2\} \end{aligned} \quad (6.8)$$

to the excess free energy density below T_c . The partition function $Z_{>}$, however, is incomplete with regard to the finite-size contributions as it does not take into account the fluctuations around the *negative* mean-field order parameter $M_{<,mf} = -[-r_0/(4u_0)]^{1/2} < 0$. A decomposition of φ_i as $\varphi_i = M_{<,mf} + \delta\varphi_i$ and an expansion of H up to $O[(\delta\varphi_i)^2]$ leads to the one-loop partition function $Z_{<}$, which is of course the same as $Z_{>}$. Thus, the total finite-size part $Z_{>}^{ex} + Z_{<}^{ex}$ of the partition function in one-loop order is then given by $2 \exp\{V \tilde{f}^{ex}\}$. The corresponding total excess free energy density is

$$\begin{aligned} f_{1\text{-loop}}^{ex,-} = & -\frac{\ln 2}{V} + \frac{1}{2V} \sum_{\mathbf{k}} \ln\{[-2(r_0 - r_{0c}) + \delta\widehat{K}(\mathbf{k})]\tilde{a}^2\} \\ & - \frac{1}{2} \int_{\mathbf{k}} \ln\{[-2(r_0 - r_{0c}) + \delta\widehat{K}(\mathbf{k})]\tilde{a}^2\}. \end{aligned} \quad (6.9)$$

Here, we have again replaced $-2r_0$ by $-2(r_0 - r_{0c})$ in the spirit of perturbation theory up to $O(1)$. The result (6.9) is identical in form with the (corrected [32]) result derived previously for cubic geometry [7]. The nonexponential finite-size term $-V^{-1} \ln 2$ is known from previous work on finite-size effects in Ising models in a block geometry of volume V [25]. Thus, this term is not specific for the $n = 1$ φ^4 theory, but rather general for systems with a twofold degeneracy of the ground state. According to the definition of the Casimir force (2.10), the constant term $-(\ln 2)/V$ in (6.9) does not contribute to F_{Casimir} .

The derivation presented above is, of course, not exact but is valid only well below T_c where the two peaks of the order-parameter distribution function at $h = 0$ are well separated and where their wings do not overlap significantly.

The evaluation of (6.9) as well as the RG treatment are parallel to that for $f_{1\text{-loop}}^{ex,+}$ above T_c . By neglecting nonasymptotic corrections to scaling, we obtain the scaling function in the scaling region well below T_c :

$$F_{1\text{-loop}}^{ex,-}(\tilde{x}, \rho) = -\rho^{d-1} \ln 2 + \frac{1}{2} \mathcal{G}_0(|2\tilde{x}|^{2\nu}, \rho) \quad (6.10)$$

with $L/\xi_- = |2\tilde{x}|^\nu$, where

$$\xi_- = \xi_{0-}|t|^{-\nu}, \quad \xi_{0-}/\xi_{0+} = 2^{-\nu} + O(u^*) \quad (6.11)$$

is the bulk second-moment correlation length below T_c and where \mathcal{G}_0 is given by (3.7). In contrast to the vanishing of $F_{1\text{-loop}}^{ex,+}$ for $\tilde{x} \rightarrow \infty$, $F_{1\text{-loop}}^{ex,-}$ approaches a *finite* value $-\rho^{d-1} \ln 2$ for $\tilde{x} \rightarrow -\infty$, as noted already in [32]. According to (6.10) and (6.3), this approach has an exponential form described by the asymptotic behavior

$$\begin{aligned} F_{\text{asympt}}^{ex,-}(\tilde{x}, \rho) = & -\rho^{d-1} \ln 2 - \left(\frac{|2\tilde{x}|^\nu}{2\pi} \right)^{\frac{d-1}{2}} \exp(-|2\tilde{x}|^\nu) \\ & - \rho^d (d-1) \left(\frac{|2\tilde{x}|^\nu}{2\pi} \right)^{\frac{d-1}{2}} \exp(-|2\tilde{x}|^\nu), \end{aligned} \quad (6.12)$$

apart from corrections of $O(e^{-2|2\tilde{x}|^\nu}, e^{-2|2\tilde{x}|^\nu})$.

The corresponding scaling functions $\Phi_{1\text{-loop}}^{ex,-}$, $X_{1\text{-loop}}^-$, $\Xi_{1\text{-loop}}^-$ and $\Phi_{\text{asympt}}^{ex,-}$, X_{asympt}^- , Ξ_{asympt}^- follow from (6.10), (6.12), (2.29), (2.40), and (2.41), respectively.

As noted above, the constant term $-\rho^{d-1} \ln 2$ does not contribute to X . This explains why the perturbation result for X of Sec. V (as shown in Fig. 12) is in better agreement with the MC data below T_c than the corresponding result for F^{ex} shown in Fig. 11. Thus, in contrast to $F^{ex,-}$ which has a *finite* low-temperature limit $-\rho^{d-1} \ln 2$, our theory predicts that the Casimir force scaling function has an exponential decay toward zero for $\tilde{x} \rightarrow -\infty$. From (6.12) and (2.29), we obtain

$$\begin{aligned} X_{\text{asympt}}^-(\tilde{x}, \rho) = & -\left(\frac{d-1}{2} + |2\tilde{x}|^\nu \right) \left(\frac{|2\tilde{x}|^\nu}{2\pi} \right)^{\frac{d-1}{2}} \exp(-|2\tilde{x}|^\nu) \\ & + \rho^d (d-1) \left(\frac{|2\tilde{x}|^\nu}{2\pi} \right)^{\frac{d-1}{2}} \exp(-|2\tilde{x}|^\nu). \end{aligned} \quad (6.13)$$

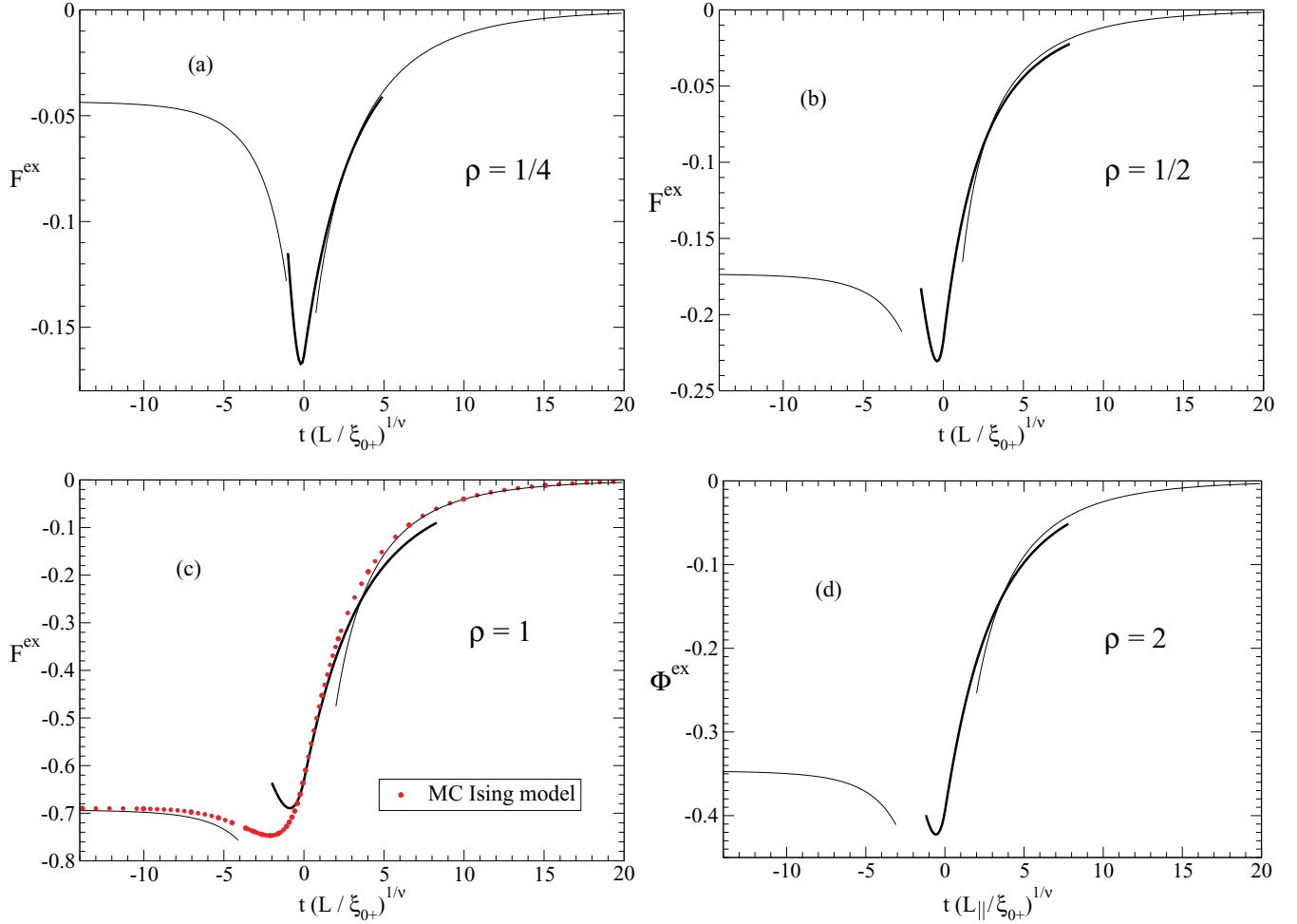


FIG. 13. (Color online) Scaling functions $F^{\text{ex}}(\tilde{x}, \rho)$ (a)–(c) and $\Phi^{\text{ex}}(\tilde{x}_{\parallel}, \rho)$ (d) as a function of $\tilde{x} = t(L/\xi_{0+})^{1/\nu}$ and $\tilde{x}_{\parallel} = t(L_{\parallel}/\xi_{0+})^{1/\nu}$, respectively, for $n = 1$ in three dimensions for several values of the aspect ratio ρ . Thick lines: improved perturbation theory according to (4.55) and (2.40). Thin lines: one-loop perturbation theory according to (6.2) and (6.10). The thin lines diverge for $t \rightarrow 0$. The asymptotic value of the thin lines is $-\rho^2 \ln 2$ for $\tilde{x} \rightarrow -\infty$ in (a)–(c) and $-(1/2) \ln 2$ for $\tilde{x}_{\parallel} \rightarrow -\infty$ in (d). MC data in (c) for the $d = 3$ Ising model by Hasenbusch [36].

It is suggestive to expect that the formulas (6.3), (6.12), and (6.13) are applicable even to $(d = 2)$ -dimensional systems. It would be interesting to check this point for the example of the two-dimensional Ising model with periodic BC in rectangular geometry.

C. Predictions for the whole scaling region

On the basis of the three perturbation results (4.55), (6.2), and (6.10), we are now in the position to present quantitative predictions for the various scaling functions over the whole range of the scaling variables $-15 \lesssim \tilde{x} \lesssim 20$ and $-15 \lesssim \tilde{x}_{\parallel} \lesssim 20$. These scaling functions are shown in Figs. 13 and 14 for various values of the aspect ratio ρ in three dimensions.

The thin lines are based on one-loop perturbation theory (6.2) and (6.10) and are applicable only away from T_c outside the central finite-size regime. For $T \rightarrow T_c$, one-loop perturbation theory breaks down, which implies that the thin lines diverge for $t \rightarrow 0$. The thick lines are based on our

lowest-mode separation approach presented in Secs. IV and V, which is applicable to the central finite-size regime including $T = T_c$. This improved perturbation approach provides a bridge through $T = T_c$ between the simple finite-size critical behavior represented by the thin lines well away from T_c . The lowest-mode separation approach is not applicable, however, to the regions $|\tilde{x}| \gg 1$ and $|\tilde{x}_{\parallel}| \gg 1$. Our Figs. 13 and 14 demonstrate that one-loop perturbation theory and improved perturbation theory complement each other and match reasonably well at intermediate values of the scaling variables. No perfect matching can be expected because of missing $O(u^*)$ terms in the one-loop results. Comparison with the MC data in Figs. 13 and 14 shows that the improvement achieved by the one-loop results is clearly visible in the range $\tilde{x} > 4$ and $\tilde{x} < -1$ [in Fig. 13(c)] and in the range $\tilde{x} < -2$ [in Fig. 14(a)]. On the whole, we consider the good agreement of our theory with the MC data over the entire scaling regime $-15 \lesssim \tilde{x} \lesssim 20$ as a major success of our strategy employing three different perturbation approaches.

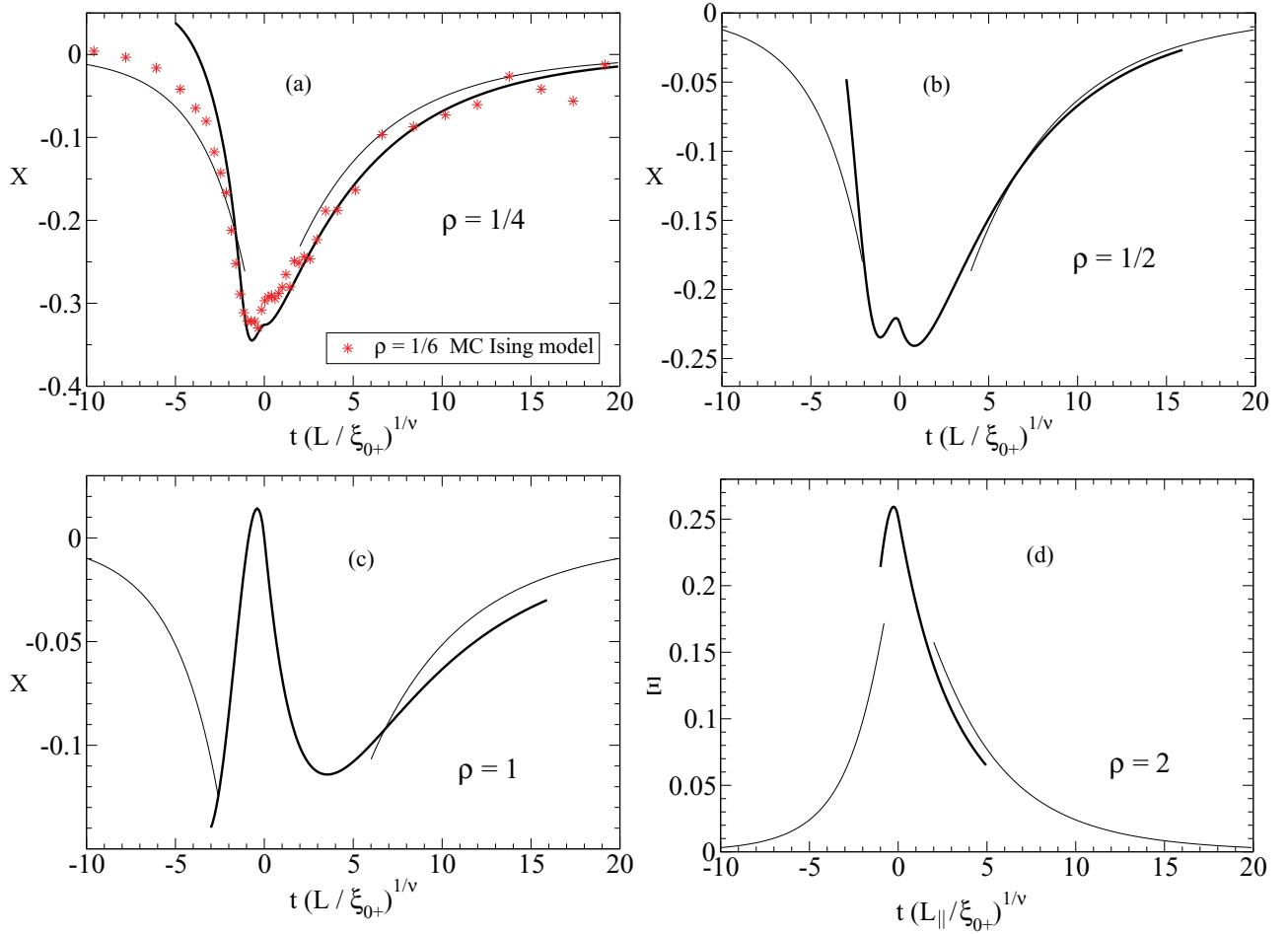


FIG. 14. (Color online) Scaling functions $X(\tilde{x}, \rho)$ (a)–(c) and $\Xi(\tilde{x}_{\parallel}, \rho)$ (d) as a function of $\tilde{x} = t(L/\xi_{0+})^{1/\nu}$ and $\tilde{x}_{\parallel} = t(L_{\parallel}/\xi_{0+})^{1/\nu}$, respectively, for $n = 1$ in three dimensions for several values of the aspect ratio ρ . Thick lines: improved perturbation theory according to (4.55), (2.29), and (2.41). Thin lines: one-loop perturbation theory according to (6.2) and (6.10). The thin lines diverge for $t \rightarrow 0$. MC data in (a) for the $d = 3$ Ising model with $\rho = 1/6$ by Vasilyev *et al.* [16].

Comparison with MC data for other values of ρ would be interesting.

D. Exponential nonscaling region

So far, we have eliminated the dependence on the lattice spacing \tilde{a} by taking the continuum limit. In earlier work, it was pointed out for confined systems in an L^d geometry [7,46] and in film geometry [8] that the finite lattice constant \tilde{a} becomes non-negligible in the limit of large L/\tilde{a} at fixed $T \neq T_c$ in the regime where the finite-size scaling function has an exponential form. The same arguments apply to the present system in a finite-block geometry. As shown in the Appendix, the excess free energy density in one-loop order attains the following form in the limit of large L/\tilde{a} , large L_{\parallel}/\tilde{a} , large L/ξ_{\pm} , and large L_{\parallel}/ξ_{\pm} :

$$f_{\text{asympt}}^{\text{ex},+} = \mathcal{A}_+(\xi_+, L, L_{\parallel}, \tilde{a}), \quad (6.14)$$

$$f_{\text{asympt}}^{\text{ex},-} = -\frac{\ln 2}{V} + \mathcal{A}_-(\xi_-, L, L_{\parallel}, \tilde{a}), \quad (6.15)$$

with the nonuniversal function

$$\begin{aligned} \mathcal{A}_{\pm}(\xi_{\pm}, L, L_{\parallel}, \tilde{a}) = & -\frac{1}{L^d} \left[1 + \left(\frac{\tilde{a}}{2\xi_{\pm}} \right)^2 \right]^{\frac{d-1}{4}} \left(\frac{L}{2\pi\xi_{\pm}} \right)^{\frac{d-1}{2}} \\ & \times \exp \left\{ \frac{L}{\xi_{\pm}} \right\} - \frac{d-1}{L^d} \left[1 + \left(\frac{\tilde{a}}{2\xi_{\pm}} \right)^2 \right]^{\frac{d-1}{4}} \\ & \times \left(\frac{L_{\parallel}}{2\pi\xi_{\pm}} \right)^{\frac{d-1}{2}} \exp \left\{ -\frac{L_{\parallel}}{\xi_{\pm}} \right\}, \end{aligned} \quad (6.16)$$

where

$$\xi_{e\pm} = \frac{\tilde{a}}{2} \left[\text{arcsinh} \left(\frac{\tilde{a}}{2\xi_{\pm}} \right) \right]^{-1} \quad (6.17)$$

are the *exponential* (“true”) bulk correlation lengths [7,33,34] above (+) and below (−) T_c , respectively. This result applies to the regions well below the dashed lines in Fig. 2, including the shaded regions. Note that no condition is imposed on the value of $0 < \tilde{a}/\xi_{\pm} < \infty$ other than that L/ξ_{\pm} and L_{\parallel}/ξ_{\pm} are

large. For $L = L_{\parallel}$, (6.16) reduces to the previous result for cubic geometry [7,50]. As a nontrivial relation between bulk properties and finite-size effects [33], the lengths ξ_{\pm} describe the exponential part of the *bulk* order-parameter correlation function [34] in the large-distance limit in the direction of one of the cubic axes at arbitrary fixed $T \neq T_c$ above and below T_c (for $n = 1$), respectively. This relation is exact in the large- n limit above T_c [33].

It has been shown [7,46] that, because of the exponential structure of the function \mathcal{A}_{\pm} , the \tilde{a} dependence of ξ_{\pm} can not be neglected even for small $\tilde{a}/\xi_{\pm} \ll 1$ if

$$L \gtrsim 24\xi_{\pm}^3/\tilde{a}^2, \quad L_{\parallel} \gtrsim 24\xi_{\pm}^3/\tilde{a}^2 \quad (6.18)$$

are sufficiently large. The conditions (6.18) follow from the second term in the expansion of the function (6.17) for small \tilde{a}/ξ_{\pm} :

$$\xi_{\pm} = \xi_{\pm} \left[1 - \frac{1}{24} \left(\frac{\tilde{a}}{\xi_{\pm}} \right)^2 + \dots \right] \quad (6.19)$$

appearing in the exponential parts of the function $\mathcal{A}_{\pm}(\xi_{\pm}, L, L_{\parallel}, \tilde{a})$ (see also [33,46]). The second term in (6.19) is *not* negligible even for small $\tilde{a}/\xi_{\pm} \ll 1$ if the conditions (6.18) are satisfied. This implies that finite-size scaling and universality are violated in the large- $|\tilde{x}|$ and large- $|\tilde{x}_{\parallel}|$ tail of $L^d f_s^{ex}$ at any $\tilde{a}/\xi_{\pm} > 0$ even arbitrarily close to T_c because, ultimately, for $|\tilde{x}| \rightarrow \infty$ and $|\tilde{x}_{\parallel}| \rightarrow \infty$ (i.e., for large L and L_{\parallel} at fixed $|t| > 0$), the tail of $L^d f_s^{ex}$ becomes explicitly dependent on \tilde{a} . As shown in Sec. X of [7], the tail depends even on the bare four-point coupling u_0 through ξ_{\pm} ; strictly speaking, it is even necessary to keep the complete nonasymptotic (u_0 -dependent) form of ξ_{\pm} at finite \tilde{a} . Thus, no \tilde{a} -independent finite-scaling form with a single scaling argument $\propto tL^{1/\nu}$ can be defined in this exponential large- $|\tilde{x}|$ and large- $|\tilde{x}_{\parallel}|$ regions. Higher-loop contributions can not remedy this violation. The same reservations apply, of course, to the critical Casimir force and its scaling form.

Note added in proof. The predictions of this paper and of Refs. [7,32] are in good agreement with recent Monte Carlo data for the three-dimensional Ising model by Hucht *et al.* [51].

ACKNOWLEDGMENTS

I am grateful to M. Hasenbusch for providing the MC data of Ref. [36] in numerical form prior to publication. I also thank A. Hucht and B. Kastening for useful discussions and correspondence.

APPENDIX: GAUSSIAN FREE ENERGY

We consider the Gaussian model, i.e., the Hamiltonian (2.1) for $u_0 = 0$, and calculate the excess free energy density in a rectangular $L_{\parallel}^{d-1} \times L$ geometry. This calculation will lead to the evaluation of the sums in (3.1) and (3.2) as well as to the derivation of (4.23)–(4.27), (6.2), (6.3), (6.10), (6.12), and (6.16). Since the calculation is largely parallel to that of [7], we skip some of the details of the derivation.

The Gaussian excess free energy density per component divided by $k_B T$ is $f_{\text{Gauss}}^{ex} = \frac{1}{2} \Delta(r_0, L_{\parallel}, L, K_{i,j}, \tilde{a})$,

$$\Delta(r_0, L_{\parallel}, L, K_{i,j}, \tilde{a}) = V^{-1} \sum_{\mathbf{k}} \ln\{[r_0 + \delta\hat{K}(\mathbf{k})]\tilde{a}^2\} - \int_{\mathbf{k}} \ln\{[r_0 + \delta\hat{K}(\mathbf{k})]\tilde{a}^2\}, \quad (A1)$$

where the sum $\sum_{\mathbf{k}}$ and the integral $\int_{\mathbf{k}}$ have finite cutoffs $\pm\pi/\tilde{a}$ for each k_{α} . Using the Poisson identity [33,47], we obtain the exact representation

$$\begin{aligned} \Delta(r_0, L_{\parallel}, L, K_{i,j}, \tilde{a}) &= - \int_0^{\infty} dy y^{-1} e^{-r_0 \tilde{a}^2 y} \sum'_{\mathbf{m}, n} \int_{\mathbf{q}} \int_p \\ &\times \exp\{-\delta\hat{K}(\mathbf{q}, p)\tilde{a}^2 y + i\mathbf{q} \cdot \mathbf{m} L_{\parallel} + ipnL\} \end{aligned} \quad (A2)$$

with $\mathbf{q} \cdot \mathbf{m} = \sum_{\alpha=1}^{d-1} q_{\alpha} m_{\alpha}$, where $\sum'_{\mathbf{m}, n}$ means summation over all integers $\mathbf{m} = (m_1, m_2, \dots, m_{d-1})$ and n without the single term with $\mathbf{m} = \mathbf{0}$, $n = 0$. In the following, we evaluate Δ for $L \gg \tilde{a}$ and $L_{\parallel} \gg \tilde{a}$ in two regimes.

1. Central finite-size regime

We assume large L/\tilde{a} , large L_{\parallel}/\tilde{a} , small $0 < r_0^{1/2}\tilde{a} \ll 1$, and fixed $0 < Lr_0^{1/2} \lesssim O(1)$, $0 < L_{\parallel}r_0^{1/2} \lesssim O(1)$, which we refer to as the central finite-size regime. In this regime, the large- (\mathbf{q}, p) dependence of $\delta\hat{K}(\mathbf{q}, p)$ does not matter. Therefore, we may replace $\delta\hat{K}(\mathbf{q}, p)$ by its long-wavelength form (2.20) and let the integration limits of $\int_{\mathbf{q}}$ and of \int_p go to ∞ . This leads to the scaling form of the Gaussian excess free energy

$$f_{\text{Gauss}}^{ex} = \frac{1}{2} \Delta(r_0, L_{\parallel}, L) = \frac{1}{2} L^{-d} \mathcal{G}_0(r_0 L^2, \rho), \quad (A3)$$

where $\mathcal{G}_j(r_0 L^2, \rho)$ is defined in (3.7). Interpreting (A3) as a one-loop contribution of the φ^4 model and applying the renormalization procedure parallel to that described in Sec. XA of [7], we arrive at the one-loop scaling function presented in (6.2).

The function $\mathcal{G}_0(r_0 L^2, \rho)$ diverges for $r_0 L^2 \rightarrow 0$, which comes from the large- z behavior of $K(z) \approx 1$ in the last term $[\rho K(\rho^2 z)]^{d-1} K(z) \approx \rho^{d-1}$ of the integrand of (3.7). We find

$$\mathcal{G}_0(r_0 L^2, \rho) \approx \rho^{d-1} \ln \left(\frac{r_0 L^2}{4\pi^2} \right) + \mathcal{C}_0(\rho) \quad (A4)$$

for $r_0 L^2 \ll 1$. In order to determine the constant $\mathcal{C}_0(\rho)$, we add and subtract the divergent term $\rho^{d-1} \ln[r_0 L^2/(4\pi^2)]$ by rewriting $\mathcal{G}_0(r_0 L^2, \rho)$ in the form

$$\begin{aligned} \mathcal{G}_0(r_0 L^2, \rho) &= \rho^{d-1} \ln \left(\frac{r_0 L^2}{4\pi^2} \right) \\ &+ \int_0^{\infty} \frac{dz}{z} \left[\exp \left(-\frac{r_0 L^2 z}{4\pi^2} \right) \left\{ \left(\frac{\pi}{z} \right)^{d/2} \right. \right. \\ &\left. \left. - [\rho K(\rho^2 z)]^{d-1} K(z) + \rho^{d-1} \right\} - \rho^{d-1} e^{-z} \right]. \end{aligned} \quad (A5)$$

The integral in (A5) has a finite limit for $r_0 L^2 \rightarrow 0$, which yields the constant

$$C_0(\rho) = \int_0^\infty \frac{dz}{z} \left[\left(\frac{\pi}{z} \right)^{d/2} - [\rho K(\rho^2 z)]^{d-1} K(z) + \rho^{d-1} (1 - e^{-z}) \right]. \quad (\text{A6})$$

Equation (A4) implies that the function

$$\mathcal{G}_1(r_0 L^2, \rho) = -\frac{\partial \mathcal{G}_0(r_0 L^2, \rho)}{\partial (r_0 L^2)} \quad (\text{A7})$$

has the divergent behavior

$$\mathcal{G}_1(r_0 L^2, \rho) \approx -\frac{\rho^{d-1}}{r_0 L^2} \quad (\text{A8})$$

for $r_0 L^2 \ll 1$. The asymptotic behavior (A4) and (A8) is needed in the discussion of the low-temperature limit in Sec. III C.

The function $\mathcal{G}_0(r_0 L^2, \rho)$ decays exponentially for large $r_0 L^2 \gg 1$. From (A16), we obtain, for $r_0 \tilde{a}^2 \ll 1$ and $r_0 L^2 \gg 1$,

$$\begin{aligned} \mathcal{G}_0(r_0 L^2, \rho) &\approx -2 \left(\frac{r_0 L^2}{4\pi^2} \right)^{(d-1)/4} \exp(-L r_0^{1/2}) \\ &\quad - 2(d-1) \rho^d \left(\frac{r_0 L^2}{4\pi^2 \rho^2} \right)^{(d-1)/4} \exp(-L r_0^{1/2} / \rho). \end{aligned} \quad (\text{A9})$$

For $\rho = 1$, Eq. (A9) agrees with Eq. (10.12) of [7].

The result (A3) is sufficient to derive the higher-mode sums $S_i(r_{0L}, L, \rho)$, (4.11), and (4.12) in the central finite-size regime. We obtain

$$\begin{aligned} &\frac{1}{V} \sum_{\mathbf{k} \neq 0} \ln[r_0 + \delta \hat{K}(\mathbf{k}) \tilde{a}^2] \\ &= \int_{\mathbf{k}} \ln[r_0 + \delta \hat{K}(\mathbf{k}) \tilde{a}^2] + \frac{1}{L^d} \ln \left(\frac{L^2}{\tilde{a}^2 4\pi^2} \right) \\ &\quad + \frac{1 - \rho^{d-1}}{L^d} \ln(r_0 \tilde{a}^2) + \frac{1}{L^d} J_0(r_0 L^2, \rho) \end{aligned} \quad (\text{A10})$$

with $J_0(x^2, \rho)$ defined by (4.26). By means of differentiation with respect to r_0 , we obtain, from (A10) for $m = 1, 2$,

$$\begin{aligned} &V^{-1} \sum_{\mathbf{k} \neq 0} [r_0 + \delta \hat{K}(\mathbf{k})]^{-m} \\ &= \int_{\mathbf{k}} [r_0 + \delta \hat{K}(\mathbf{k})]^{-m} + \frac{1 - \rho^{d-1}}{L^d} (r_0)^{-m} \\ &\quad + \frac{L^{2m-d}}{(4\pi^2)^m} I_m(r_0 L^2, \rho) \end{aligned} \quad (\text{A11})$$

with $I_m(r_0 L^2, \rho)$ defined by (4.27). For the bulk integrals, see [7].

2. Exponential regime above T_c

Now we assume $L r_0^{1/2} \gg 1$ and $L_{\parallel} r_0^{1/2} \gg 1$ at finite $\rho = L/L_{\parallel}$ for fixed $r_0^{1/2} \tilde{a} > 0$, which we refer to as the exponential regime since $\Delta(r_0, L_{\parallel}, L, K_{i,j}, \tilde{a})$ will attain an exponential

L and L_{\parallel} dependence in this regime. In this regime, the complete \mathbf{k} dependence of the microscopic interaction $\delta \hat{K}(\mathbf{k})$ does matter. We use the nearest-neighbor interaction (2.19) in the form

$$\delta \hat{K}(\mathbf{q}, p) = \frac{2}{\tilde{a}^2} \sum_{\alpha=1}^{d-1} [1 - \cos(\tilde{a} q_{\alpha})] + \frac{2}{\tilde{a}^2} [1 - \cos(\tilde{a} p)]. \quad (\text{A12})$$

By generalizing the derivation of [7] to block geometry, we obtain, for large L/\tilde{a} and L_{\parallel}/\tilde{a} but arbitrary $\tilde{r}_0 \equiv r_0 \tilde{a}^2 > 0$ (compatible with $L r_0^{1/2} \gg 1$ and $L_{\parallel} r_0^{1/2} \gg 1$),

$$\begin{aligned} &\Delta(r_0, L_{\parallel}, L, K_{i,j}, \tilde{a}) \\ &= -\frac{2}{\tilde{a}^d (2\pi L/\tilde{a})^{d/2}} \int_0^\infty dz \frac{\exp[\Phi(z, \tilde{r}_0) L/\tilde{a}]}{z^{(d+1)/2} q^{1/2}} \\ &\quad - \frac{2(d-1)}{\tilde{a}^d (2\pi L_{\parallel}/\tilde{a})^{d/2}} \int_0^\infty dz \frac{\exp[\Phi(z, \tilde{r}_0) L_{\parallel}/\tilde{a}]}{z^{(d+1)/2} q^{1/2}}, \end{aligned} \quad (\text{A13})$$

where $q = (1 + z^2)^{1/2}$ with

$$\Phi(z, \tilde{r}_0) = -(1 + \tilde{r}_0/2)z + q + \ln \left(\frac{z}{1+q} \right). \quad (\text{A14})$$

The maximum of the function $\Phi(z, \tilde{r}_0)$ in the exponential parts of the integrand of (A13) is at $z = \bar{z}$, where

$$\bar{z} = \left[\tilde{r}_0 \left(1 + \frac{\tilde{r}_0}{4} \right) \right]^{-1/2}. \quad (\text{A15})$$

By expanding $\Phi(z, \tilde{r}_0)$ around $z = \bar{z}$ up to $O[(z - \bar{z})^2]$ and performing the integration over z , we finally obtain the Gaussian excess free energy density, for large L/\tilde{a} and large L_{\parallel}/\tilde{a} at arbitrary fixed $r_0 > 0$,

$$\begin{aligned} f_{\text{Gauss, asymp}}^{\text{ex}} &= -\frac{1}{L^d} \left(\frac{L/\tilde{a}}{2\pi \bar{z}} \right)^{(d-1)/2} e^{-L/\xi_{\epsilon}^G} \\ &\quad - \frac{(d-1)}{L_{\parallel}^d} \left(\frac{L_{\parallel}/\tilde{a}}{2\pi \bar{z}} \right)^{(d-1)/2} e^{-L_{\parallel}/\xi_{\epsilon}^G} \end{aligned} \quad (\text{A16})$$

with the *exponential* (“true”) bulk correlation length of the Gaussian model

$$\xi_{\epsilon}^G = \frac{\tilde{a}}{2} \left[\text{arcsinh} \left(\frac{r_0^{1/2} \tilde{a}}{2} \right) \right]^{-1}. \quad (\text{A17})$$

We recall that $r_0^{-1/2} = \xi_{+}^G$ is the *second-moment* bulk correlation length of the Gaussian model above T_c . For $L = L_{\parallel}$ (cube), (A16) yields the previous result of Eq. (B24) of [7]. No universal finite-size scaling function of the Gaussian model can be defined in the region $L \gtrsim 24(\xi_{+}^G)^3/\tilde{a}^2$ and $L_{\parallel} \gtrsim 24(\xi_{+}^G)^3/\tilde{a}^2$ because of the explicit \tilde{a} dependence of (A16) and (A17).

Within a RG treatment of the ϕ^4 lattice model, the Gaussian results (A3) and (A16) can be considered as the bare one-loop contributions to the excess free energy density. By means of such a RG treatment at finite lattice constant \tilde{a} parallel to Sec. 2 and Appendix of [46], these results acquire the correct critical exponents of the $n = 1$ universality class, including corrections to scaling. This leads to the one-loop results at finite \tilde{a} in Sec. VI D.

- [1] M. E. Fisher and P. G. de Gennes, *C. R. Seances Acad. Sci. Ser. B* **287**, 207 (1978).
- [2] For reviews, see M. Krech, *The Casimir Effect in Critical Systems* (World Scientific, Singapore, 1994); *J. Phys. Condens. Matter* **11**, R391 (1999); A. Gambassi, *J. Phys.: Conf. Ser.* **161**, 012037 (2009).
- [3] G. A. Williams, *Phys. Rev. Lett.* **92**, 197003 (2004); **95**, 259702 (2005); T. Schneider, in *The Physics of Superconductors*, edited by K. H. Bennemann and J. B. Ketterson, Vol. II (Springer, Berlin, 2004), p. 111.
- [4] V. Privman, A. Aharony, and P. C. Hohenberg, in *Phase Transitions and Critical Phenomena*, edited by C. Domb and J. L. Lebowitz, Vol. 14 (Academic, New York, 1991), p. 1.
- [5] X. S. Chen and V. Dohm, *Phys. Rev. E* **70**, 056136 (2004).
- [6] V. Dohm, *J. Phys. A: Math. Gen.* **39**, L259 (2006).
- [7] V. Dohm, *Phys. Rev. E* **77**, 061128 (2008); **79**, 049902(E) (2009).
- [8] B. Kastening and V. Dohm, *Phys. Rev. E* **81**, 061106 (2010).
- [9] D. Dantchev and D. Grüneberg, *Phys. Rev. E* **79**, 041103 (2009).
- [10] A violation of two-scale factor universality due to anisotropy was also noted by X. S. Chen and H. Y. Zhang, *Int. J. Mod. Phys. B* **21**, 4212 (2007) in the context of the correlation length and by W. Selke, *Eur. Phys. J. B* **51**, 223 (2006), in the context of the Binder cumulant. For a discussion of anisotropy effects see also H. W. Diehl and H. Chamati, *Phys. Rev. B* **79**, 104301 (2009). For a response to this discussion, see [8].
- [11] It has been proposed by Williams [3] that measurable effects caused by the critical Casimir force may exist in anisotropic superconducting films. In a comment on [3] by D. Dantchev, M. Krech, and S. Dietrich, *Phys. Rev. Lett.* **95**, 259701 (2005), the measurability of the critical Casimir force in superconductors proposed in [3] has not been questioned. This is in contrast to the opinion expressed in [12] that “the critical Casimir force is only active in fluid systems.” We disagree with this claim. An appropriately defined critical Casimir force may well be active in nonfluid systems not only because of the proposal presented in [3], but also for the following reason. Consider, for example, magnetic systems near the Curie (or Néel) point [13], solids near a structural phase transition of second order [14], or alloys near an order disorder transition of second order [15], where critical fluctuations of the order parameter are coupled to the lattice degrees of freedom (elastic modes, phonon modes). This implies the existence of long-range correlations of the lattice degrees of freedom near T_c , which are sensitive to the characteristic length L of the system, e.g., the thickness L of a slab [Fig. 1(a)]. This causes an L dependence of the free energy, which in turn causes an L -dependent thermodynamic Casimir force [as defined by Eq. (2.11) in Sec. II of this paper] that has an influence on the elastic degrees of freedom. More specifically, it should cause an L -dependent macroscopic distortion of the lattice, which is, in principle, an observable phenomenon. So far, no theoretical estimates or MC simulations on this finite-size effect are available near criticality since previous studies on the critical Casimir force [2,12,16] are based on idealized rigid-lattice model systems with zero compressibility, where the length L and the number of particles of the system were not treated as independent thermodynamic variables.
- [12] F. Parisen Toldin and S. Dietrich, *J. Stat. Mech.* (2010) P11003.
- [13] Both first- and second-order transitions may occur in compressible magnetic systems depending on boundary conditions, number n of components of the order parameter, anisotropies, range of interactions, and constraints, as discussed by D. J. Bergman and B. I. Halperin, *Phys. Rev. B* **13**, 2145 (1976) and references therein. If a first-order transition occurs, one can nevertheless observe critical behavior in a range of temperatures before the transition if the discontinuity at the first-order transition is very small, which is usually the case, as noted by Bergman and Halperin.
- [14] A. D. Bruce and R. A. Cowley, *Structural Phase Transitions* (Taylor & Francis, London, 1981); E. K. H. Salje, *Phase Transitions in Ferroelastic and Co-Elastic Crystals* (Cambridge University, Cambridge, UK, 1990); E. K. H. Salje, *Phys. Rep.* **215**, 49 (1992).
- [15] A. Onuki, *Phase Transition Dynamics* (Cambridge University, Cambridge, UK, 2002).
- [16] O. Vasilyev, A. Gambassi, A. Maciolek, and S. Dietrich, *Europhys. Lett.* **80**, 60009 (2007); *Phys. Rev. E* **79**, 041142 (2009); **80**, 039902(E) (2009).
- [17] K. Binder, *Z. Phys. B: Condens. Matter* **43**, 119 (1981).
- [18] W. Selke and L. N. Shchur, *J. Phys. A: Math. Gen.* **38**, L739 (2005); *Phys. Rev. E* **80**, 042104 (2009). See, also, M. Schulte and C. Drope, *Int. J. Mod. Phys. C* **16**, 1217 (2005); M. A. Sumour, D. Stauffer, M. M. Shabat, and A. H. El-Astal, *Phys. A (Amsterdam)* **368**, 96 (2006); V. Dohm, *Physik Journal* **8**(11), 37 (2009); J. Rudnick, R. Zandi, A. Shackell, and D. Abraham, *Phys. Rev. E* **82**, 041118 (2010); W. Selke, *ibid.* **83**, 042102 (2011).
- [19] M. Krech and S. Dietrich, *Phys. Rev. A* **46**, 1886 (1992); **46**, 1922 (1992).
- [20] H. W. Diehl, D. Grüneberg, and M. A. Shpot, *Europhys. Lett.* **75**, 241 (2006).
- [21] D. Grüneberg and H. W. Diehl, *Phys. Rev. B* **77**, 115409 (2008).
- [22] D. Dantchev and M. Krech, *Phys. Rev. E* **69**, 046119 (2004).
- [23] In Fig. 15 of [16], the location of the film transition for the 3d Ising model with isotropic interactions is indicated at the value $x^* = -1.6$ of the scaling variable x , slightly below the minimum. Note that the value of x^* is universal only for isotropic systems, whereas it is expected to be nonuniversal for anisotropic systems [8].
- [24] A brief account of our approach has been given in V. Dohm, *Europhys. Lett.* **86**, 20001 (2009).
- [25] V. Privman and M. E. Fisher, *J. Stat. Phys.* **33**, 385 (1983).
- [26] V. Dohm, *Phys. Scr. T* **49**, 46 (1993).
- [27] F. M. Gasparini, M. O. Kimball, K. P. Mooney, and M. Diaz-Avila, *Rev. Mod. Phys.* **80**, 1009 (2008).
- [28] J. Rudnick, H. Guo, and D. Jasnow, *J. Stat. Phys.* **41**, 353 (1985).
- [29] E. Brézin and J. Zinn-Justin, *Nucl. Phys. B* **257**, 867 (1985).
- [30] A. Esser, V. Dohm, M. Hermes, and J. S. Wang, *Z. Phys. B: Condens. Matter* **97**, 205 (1995).
- [31] A. Esser, V. Dohm, and X. S. Chen, *Phys. A (Amsterdam)* **222**, 355 (1995).
- [32] V. Dohm, *Phys. Rev. E* **82**, 029902(E) (2010).
- [33] X. S. Chen and V. Dohm, *Eur. Phys. J. B* **15**, 283 (2000).
- [34] M. E. Fisher and R. J. Burford, *Phys. Rev.* **156**, 583 (1967).
- [35] V. Dohm, *Z. Phys. B: Condens. Matter* **60**, 61 (1985); **61**, 193 (1985); R. Schloms and V. Dohm, *Nucl. Phys. B* **328**, 639 (1989); *Phys. Rev. B* **42**, 6142 (1990).

- [36] M. Hasenbusch (private communication).
- [37] V. Privman and M. E. Fisher, *Phys. Rev. B* **30**, 322 (1984).
- [38] H. W. Diehl and D. Grüneberg, *Nucl. Phys. B* **822**, 517 (2009); M. Burgsmüller, H. W. Diehl, and M. A. Shpot, *J. Stat. Mech.* (2010) P11020.
- [39] A. Onuki and A. Minami, *Phys. Rev. B* **76**, 174427 (2007).
- [40] D. Danchev, *Phys. Rev. E* **53**, 2104 (1996).
- [41] K. K. Mon, *Phys. Rev. Lett.* **54**, 2671 (1985); *Phys. Rev. B* **39**, 467 (1989).
- [42] V. Dohm, *Z. Phys. B: Condens. Matter* **75**, 109 (1989).
- [43] H. J. Krause, R. Schloms, and V. Dohm, *Z. Phys. B: Condens. Matter* **79**, 287 (1990).
- [44] S. A. Larin, M. Mönnigmann, M. Strösser, and V. Dohm, *Phys. Rev. B* **58**, 3394 (1998).
- [45] A. J. Liu and M. E. Fisher, *Phys. A (Amsterdam)* **156**, 35 (1989).
- [46] X. S. Chen and V. Dohm, *Eur. Phys. J. B* **10**, 687 (1999).
- [47] P. M. Morse and H. Feshbach, *Methods of Theoretical Physics* (McGraw-Hill, New York, 1953).
- [48] K. Binder and D. P. Landau, *Phys. Rev. B* **30**, 1477 (1984).
- [49] X. S. Chen and V. Dohm, *Phys. A (Amsterdam)* **235**, 555 (1997); *Int. J. Mod. Phys. B* **12-13**, 1277 (1998).
- [50] The exponent $d - 1$ of the first square bracket of Eq. (10.15) of [7] should read as $(d - 1)/4$.
- [51] A. Hucht, D. Grüneberg, and F. M. Schmidt, *Phys. Rev. E* **83**, 051101 (2011).